AD-A074 368 NAVAL RESEARCH LAB WASHINGTON DC F/G 20/5
ANALYTIC ANALYSIS OF LINEAR GROWTH RATES OF GYROTRON FOR TE(LNS--ETC(U)
JUN 79 J Y CHOE, S AHN

UNCLASSIFIED NRL-MR-4035 SBIE-AD-E000 324 NL

| OF |
AD
A074368

END
DATE
FILMED
10-79
DDC

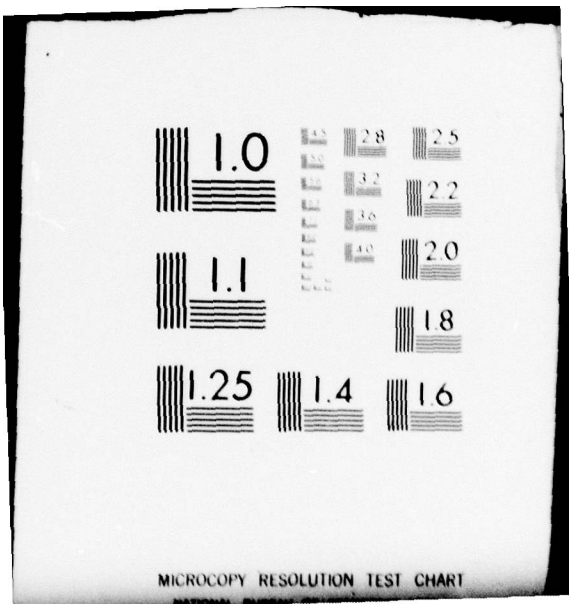
1.0
1.1
1.25
1.4
1.6
1.8
2.0
2.2
2.5
2.8
3.2
3.6
4.0
MICROCOPY RESOLUTION TEST CHART

(9) NRL Memorandum Report 4035

(6)

Analytic Analysis of Linear Growth Rates of Gyrotron for TE(lns) Mode with Zero-Temperature Beam Electrons.

(10) JOON Y. CHOE, Saeyoung Ahn

Department of Physics and Astronomy
University of Maryland

SAEYOUNG AHN

Electronics Technology Division

(11) 29 Jun 79

(12) 57p.

(14) NRL-MR-4035

(18) SBIE

June 29, 1979

(19) AD-E000 324

NAVAL RESEARCH LABORATORY
Washington, D.C.

SECURITY CLASSIFICATION OF THIS PAGE (When Data Entered)

REPORT DOCUMENTATION PAGE

READ INSTRUCTIONS BEFORE COMPLETING FORM

1. REPORT NUMBER: NRL Memorandum Report 4035
2. GOVT ACCESSION NO.
3. RECIPIENT'S CATALOG NUMBER

4. TITLE (and Subtitle): ANALYTIC ANALYSIS OF LINEAR GROWTH RATES OF GYROTRON FOR TE $_{lns}$ MODE WITH ZERO-TEMPERATURE BEAM ELECTRONS
5. TYPE OF REPORT & PERIOD COVERED: Interim report on a continuing NRL problem
6. PERFORMING ORG. REPORT NUMBER

7. AUTHOR(s): Saeyoung Ahn and Joon Y. Choe*
8. CONTRACT OR GRANT NUMBER(s)

9. PERFORMING ORGANIZATION NAME AND ADDRESS: Naval Research Laboratory, Washington, D.C. 20375
10. PROGRAM ELEMENT, PROJECT, TASK AREA & WORK UNIT NUMBERS: NRL 52R18-35

11. CONTROLLING OFFICE NAME AND ADDRESS
12. REPORT DATE: June 29, 1979
13. NUMBER OF PAGES: 56

14. MONITORING AGENCY NAME & ADDRESS(if different from Controlling Office)
15. SECURITY CLASS. (of this report): Unclassified
15a. DECLASSIFICATION/DOWNGRADING SCHEDULE

16. DISTRIBUTION STATEMENT (of this Report)

Approved for public release; distribution unlimited.

17. DISTRIBUTION STATEMENT (of the abstract entered in Block 20, if different from Report)

18. SUPPLEMENTARY NOTES

*Department of Physics and Astronomy
University of Maryland

19. KEY WORDS (Continue on reverse side if necessary and identify by block number)

Gyrotron
Cyclotron maser instability
High harmonic mode
Dispersion relation
Waveguide
Electron density distribution function

20. ABSTRACT (Continue on reverse side if necessary and identify by block number)

The approximate expression for the growth rate of the transverse electric (TE) mode with the azimuthal mode number, l, the radial node number n, and the magnetic harmonic number s of the electron cyclotron maser instability with zero-tempertured beam electrons is derived and analytically examined. It has been found that there exist two branches of instabilities distinguished by their axial wavenumbers; the short and the long wavelength modes, and the estimates of their growth rates have been obtained. With maximization processes of the growth rates, the optimum

(continued)

DD FORM 1 JAN 73 1473 EDITION OF 1 NOV 65 IS OBSOLETE
S/N 0102-014-6601

SECURITY CLASSIFICATION OF THIS PAGE (When Data Entered)

20. Abstract (continued)

conditions on various parameters have been found. In particular, it has been found that $s = 1$ mode with the beam center coinciding with the axis yields the highest growth rate. The exponential behavior of the growth with respect to the magnetic harmonic number s is also obtained.

CONTENTS

ANALYTIC ANALYSIS OF LINEAR GROWTH RATES OF GYROTRON FOR TE_{lns} MODE WITH ZERO-TEMPERATURE BEAM ELECTRONS

I. INTRODUCTION

The general dispersion equation for transverse electric (TE) modes of the electron cyclotron maser instability was previously obtained in Ref. 1 (hereinafter referred to paper A). It is the objective of this paper to analytically examine the dispersion relation.

In the spirit of application of the cyclotron maser instability to gyrotron amplifier devices, we will identify different instability types and will find optimum conditions in experimental parameters that maximize the growth rates. The analytical expression for the growth rates is obtained with the tenuous beam approximation that is consistent with the assumption in deriving the general dispersion equation (see Chapter II in paper A).

Although the dispersion Eq. ((70) in paper A) is valid for arbitrary distribution function of beam electrons, we will restrict ourselves to zero-temperature beam, whose dispersion relation is given by Eq. 76 in paper A. Also we will consider the gyrotron with single conductor, for simplicity, even though some of the results are still valid for coaxial gyrotron devices.

The geometry of the gyrotron we consider is that of cylindrical wall within which the electron beam is passed. The cross section of the device is shown in Fig. 1. The conducting wall is located at $r = R$, and the beam electrons of constant Larmor radii, r_L are gyrating with constant guiding center radii, r_0 around constant magnetic field $B_0 \hat{e}_z$. The axial motion of electrons are

Manuscript submitted May 16, 1979.

characterized by constant velocity v_z. The distribution function describing such electrons is a δ-function given by Eq. (73) in paper A, and the resulting dispersion relation for TE_{lns} mode becomes Eq. (76) in paper A. Here mode identification integers l, n, and s represent the mode numbers for the azimuthal (θ), the radial (r) directions, and the magnetic harmonic number of Doppler-shifted cyclotron motion, respectively. In addition, the axial mode is identified by wavenumber k.

The dispersion relation eq. (76) in paper A is obtained under the tenuous beam approximation within the framework of linearized Vlasov-Maxwell equation with form of $\exp[ikz + il\theta - i\omega t]$. The tenuous beam assumptions can be written as

$$\nu/\gamma_0 << 1, \tag{1}$$

where the Budker parameter ν is defined by

$$\nu \equiv \left[\frac{Ne^2}{mc^2}\right], \tag{2}$$

and γ_0 is the total relativistic factor of the electron. Here the total number of electrons per unit axial length N is given by

$$N \equiv 2\pi \int r dr \; f_0(\gamma, p_z, P_\theta). \tag{3}$$

The procedures of deriving the dispersion relation is very complicated, and we refer details to paper A. It is sufficient to say that the tenuous beam assumption (1) allows us to neglect self-field effects, and that usage of constants of electron motion (γ, p_z, P_θ) as the coordinates for beam distribution function f_0 eliminates much of the mathematical complexity. Here the constants of motion γ, p_z and P_θ refer to the total relativistic factor of the electron, the linear momentum in axial direction, and the azimuthal canonical angular momentum.

After brief discussions of the dispersion equations in Chapter II, we identify two different types of instability (short-and long-wavelength modes), and derive approximate expressions for

their growth rates (Chapter II). From Chapter IV and on, we limit our attention to more interesting long-wavelength modes. The stability boundary is found in Section A of Chapter IV, and the estimates of growth rates and the matching conditions on wall location are obtained in Section B. Further optimization of the growth rates with respect to various parameters are given in Chapt. V.

It should be emphasized here that our intention in this paper is to obtain general tendency of the dispersion equation without help of numerical calculations. For this purpose we frequently resolve the graphic solutions.

II. DISPERSION EQUATION

The dispersion relation for TE_{lns} mode for the device described in Chapter I is given by Eq. (76) of paper A. Namely,

$$D(\omega, k) = 0, \tag{4}$$

where

$$D(\omega, k) = [\omega^2 - \omega_{ln}^2] + \frac{2c^2 \nu X_{ln}^2}{\gamma_0 R^2 N_{ln}} \left[\frac{\beta_\perp^2 H(\Omega_s^2 - c^2k^2)}{(\omega - \Omega_s)^2} - 2\frac{\left[\frac{\omega_c}{\gamma} Q - \beta_\perp^2 H \Omega_s\right]}{(\omega - \Omega_s)} - (U - \beta_\perp^2 H) \right]. \tag{5}$$

The various terms in Eq. (5) are defined by

$$\begin{aligned} \omega_{ln}^2 &\equiv c^2\left[k^2 + \frac{X_{ln}^2}{R^2}\right], \\ \Omega_s &\equiv k v_z + s\omega_c/\gamma_0, \\ N_{ln} &\equiv \frac{1}{2}(X_{ln}^2 - l^2)\, J_l^2(X_{ln}), \\ \omega_c &\equiv eB_0/mc, \\ \beta_\perp^2 &\equiv \frac{\omega_c r_L}{\gamma_0 c} = \frac{v_\perp}{c}. \end{aligned} \tag{6}$$

and the functions $H \equiv H_{sl}(X_0, X_L)$, $Q \equiv Q_{sl}(X_0, X_L)$, and $U \equiv U_{sl}(X_0, X_L)$ are given by

$$
\begin{aligned}
H_{sl}(X_0, X_L) &= [J_{s-l}(X_0) J_s'(X_L)]^2, \\
Q_{sl}(X_0, X_L) &= J_{s-l}(X_0)\, J_s'(X_L) \left[\frac{s(s^2 - X_L^2)}{X_L}\, J_{s-l}(X_0) J_s(X_L) \right. \\
&\quad \left. + \frac{X_L^2 (s-l)}{X_0}\, J_{s-l}'(X_0)\, J_s'(X_L) \right], \qquad (7) \\
U_{sl}(X_0, X_L) &= J_s(X_L)\, J_s'(X_L) \left[\left\{ \frac{(2s^2 - X_L^2)}{X_L} - \frac{X_L (s-l)^2}{X_0^2} \right\} J_{s-l}^2(X_0) \right. \\
&\quad \left. - X_L \left\{ J_{s-l}'(X_0) \right\}^2 \right].
\end{aligned}
$$

The arguments of H, Q, U are defined by

$$
\begin{aligned}
X_0 &\equiv \frac{X_{ln}}{R}\, r_0, \qquad (8) \\
X_L &\equiv \frac{X_{ln}}{R}\, r_L,
\end{aligned}
$$

where

$$
J_l'(X_{ln}) = 0. \qquad (9)
$$

The solution of Eq. (4), that is, if $D(\omega = \omega_r + i\omega_i) = 0$, determines the eigen frequency ω_r and the growth rate $|\omega_i|$ if $\omega_i \neq 0$. The first term in Eq. (5) describes free wave guide motion with eigen frequency ω_{ln}, while the second terms represents the correction to free wave guide equation due to the cyclotron motion (with frequency Ω_s) of beam electrons. It is thus the second term that gives rise to the instability with $\omega_i \neq 0$.

For systematic analysis, we normalize quantities as follows

$$
\begin{aligned}
\begin{bmatrix} \omega \\ \omega_{ln} \\ \Omega_s \end{bmatrix} &= s\omega_c/\gamma_0 \begin{bmatrix} \tilde{\omega} \\ \tilde{\omega}_{ln} \\ \tilde{\Omega}_s \end{bmatrix}, \\
R &= \frac{cX_{ln}}{\gamma_z s\omega_c/\gamma_0}\, \tilde{R}, \qquad (10) \\
r_0 &= R\, \tilde{r}_0, \\
k &= \frac{s\omega_c/\gamma_0}{c}\, \tilde{k}
\end{aligned}
$$

where the axial relativistic factor γ_z is defined by

$$\gamma_z \equiv (1 - \beta_z^2)^{-\frac{1}{2}},$$

with

$$\beta_z \equiv \frac{v_z}{c}. \tag{11}$$

With thus normalized quantities, the dispersion equation $D = 0$ can be written as

$$D(\tilde{\omega}; \tilde{k})$$

$$= [\tilde{\omega}^2 - \tilde{\omega}_{ln}^2] + \frac{A_{ln}}{\tilde{R}^2}\left[\frac{\beta_\perp^2 H(\tilde{\Omega}_s^2 - \tilde{k}^2)}{(\tilde{\omega} - \tilde{\Omega}_s)^2} - 2\frac{\left[\frac{Q}{s} - \beta_\perp^2 H\tilde{\Omega}_s\right]}{(\tilde{\omega} - \tilde{\Omega}_s)} - (U - \beta_\perp^2 H)\right] = 0, \tag{12}$$

where

$$\tilde{\omega}_{ln}^2 \equiv \tilde{k}^2 + \frac{\gamma_z^2}{\tilde{R}^2},$$

$$\tilde{\Omega}_s \equiv \tilde{k}\beta_z + 1,$$

$$A_{ln} \equiv \frac{2\nu\gamma_z^2}{\gamma_0 N_{ln}}, \tag{13}$$

$$X_L \equiv \frac{\gamma_z s}{\tilde{R}}\beta_\perp, \quad X_0 \equiv X_{ln}\tilde{r}_0$$

Here A_{ln} is small quantity, typically in the order of 10^{-3}.

The normalized dispersion function $D(\tilde{\omega}; \tilde{k})$ is convenient in that the magnetic harmonic number s is factored out except for the complicated functions, H, Q, and U. Hereinafter, we will use the normalized quantities (Eqs. (12) and (13)) with tilde dropped. When we consider the real parameters, the normalization Eq. (10) will be referred to.

The waveguide eigenfrequency ω_{ln}, and the Doppler-shifted cyclotron frequency Ω_s as functions of axial wave number are illustrated in Fig. 2. It is useful to define the following wavenumbers:

$$\Omega_s - k^2 = 0 \quad at \quad k = k_\pm^\delta, \tag{14}$$

$$\Omega_s^2 - \omega_{ln}^2 = 0 \quad at \quad k = k_{\pm}^a, \tag{15}$$

and

$$\Omega_s = 0 \quad at \quad k = k_o. \tag{16}$$

It is easy to show that, from Eq. (13),

$$k_{\pm}^b = \gamma_z^2[\beta_z \pm 1] \tag{17}$$

$$k_{\pm}^a = \gamma_z^2[\beta_z \pm (1 - 1/R^2)^{\frac{1}{2}}], \tag{18}$$

and

$$k_o = -\frac{s}{\beta_z}. \tag{19}$$

The waveguide frequency ω_{ln} is a hyperbolic function of k with the cutoff frequency $\frac{\gamma_z}{R}$ (i.e. intersection of ω_{ln} with ω-axis), and the cyclotron frequency Ω_s is a straight line of slope β_z intersecting ω-axis at 1. It is evident from Eq. (18) that for $R < 1$, ω_{ln} is always greater than Ω_s, and particularly for $R = 1$, Ω_s is tangential to ω_{ln}. Figure 2 shows an example for $R > 1$.

Before we obtain the expression for the growth rate ω_i from Eq. (12), we will first demonstrate the presence of the complex roots (i.e. $\omega_i \neq 0$) in Eq. (12). We rewrite the dispersion equation as

$$D = D_0 + D_1 + D_2 + D_3, \tag{20}$$

where

$$D_0 \equiv \omega^2 - \omega_{ln}^2, \tag{21}$$

$$D_1 \equiv \frac{\eta}{R^2} \frac{(\Omega_s^2 - k^2)}{(\omega - \Omega_s)^2} \tag{22}$$

$$D_2 \equiv -\frac{2A_{ln}}{R^2} \frac{\left[\frac{Q}{s} - \beta_{\perp}^2 H \Omega_s\right]}{(\omega - \Omega_s)}, \tag{23}$$

$$D_3 \equiv -\frac{A_{ln}}{R^2}(U - \beta_{\perp}^2 H). \tag{24}$$

Here small quantity η is defined by

$$\eta \equiv \frac{2\nu\gamma_z^2\beta_\perp^2}{\gamma_0 N_{ln}} H_{sl}(X_0, X_L), \tag{25}$$

and the typical magnitude of η is in the order of 10^{-4}.

For given parameters and k the dispersion function D is a function of ω, and the roots of $D(\omega) = 0$ will determine the eigenfrequency. In order to have growing mode, the equation $D(\omega) = 0$ must have complex roots. We note that in the absence of beam electron (i.e. $\nu = 0 = \eta$), the dispersion equation $D = 0$ becomes $D_0 = 0$. The free waveguide function $D_0(\omega)$ is a quadratic function of ω, and the free waveguide equation $D_0 = 0$ has roots at $\omega = \pm \omega_{ln}$, representing freely (without growth or attentuation, i.e. $\omega_i = 0$) travelling waveguides in opposite directions. With electrons ($\nu \neq 0$), we can easily show that, due to the resonance term $(\omega - \Omega_s)$ in denominator of D_1 and D_2, and the smallness of the coefficients of D_1, D_2, and D_3, the dispersion function $D(\omega)$ can be approximated as

$$D(\omega) \simeq D_0(\omega) \tag{26}$$

at $|\omega - \Omega_s| >> 0$, and

$$D(\omega) \simeq D_0(\omega) + D_1(\omega) \tag{27}$$

near $\omega = \Omega_s$, where the magnitudes of D_2 and D_3 are much less than that of D_1 (see Eqs. (22) - (24)). Since $D_0(\omega) = 0$ (Eq. 26) have real roots, and complex roots are possible only for $D_0(\omega) + D_1(\omega) = 0$ (Eq. 27), we conclude that instability may be present only near $\omega = \Omega_s$. We therefore examine the behavior of $D_0(\omega) + D_1(\omega)$ with respect to ω near Ω_s, which are illustrated in Figs. (3a) and (3b). At two representative values of k (noted as I and II in Fig. 2), their approximate dispersion functions $D_0(\omega) + D_1(\omega)$ with $D_0(\omega)$ for comparison purpose are drawn near $\omega = \Omega_s$ in Fig. 3(a) and (b). Note that $k^I < k_+^b < k^{II}$, and that at $k = k^I$ (Fig. 3a) $\Omega_s^I > \omega_{ln}^I$, while at $k = k^{II}$ (Fig. 3b) $\Omega_s^{II} < \omega_{ln}^{II}$. It is apparent from Fig. 3 (a) and (b) that the difference of dispersion function with electron beams ($D_0 + D_1$) from free wave

guide function (D_0) is localized near $\omega = \Omega_s$. The combined dispersion function hardly changes the free waveguide eigenfrequency ω_{ln}, while at the opposite side of Ω_s from ω_{ln}, it shows a local extremum $\left[viz.\ \frac{\partial D}{\partial \omega} = 0 \text{ and } D\frac{\partial^2 D}{\partial \omega^2} > 0\right]$. As can be seen in Appendix A, the fact that the function $D(\omega)$ has a local extremum near $\omega = \Omega_s$ means that the dispersion equation $D(\omega) = 0$ yields complex solutions ($\omega_i \neq 0$) near that point. Since imaginary part of the solution of $D(\omega) = 0$ represents the growth rate, the presence of the local extremum corresponds to instability near $\omega = \Omega_s$. The presence of the local extremum near $\omega = \Omega_s$ is due to the fact that D_1 is proportional to $(\omega - \Omega_s)^{-2}$, which yields steep slope near $\omega = \Omega_s$ and same signs as it crosses $\omega = \Omega_s$ line. We have graphically shown that the dispersion equation $D(\omega) = 0$ can have complex solutions and thereby growing modes near $\omega = \Omega_s$. In the next chapter we will find the approximate expression for the actual growth rate.

III. GROWTH RATE EQUATION

The dispersion Eq. (12) can be written as

$$\Delta^2 [(\Omega_s^2 - \omega_{ln}^2) + 2\Omega_s \Delta + \Delta^2] + \frac{A_{ln}}{R^2}\left[\beta_\perp^2 H(\Omega_s^2 - k^2) - 2\Delta\left(\frac{Q}{s} - \beta_\perp^2 H\Omega_s\right) - \Delta^2 (U - \beta_\perp^2 H)\right] = 0, \tag{29}$$

where the small frequency shift Δ is defined by

$$\Delta \equiv \omega - \Omega_s \equiv \Delta_r + i\,\Delta_i. \tag{30}$$

When the tenuous beam is assumed (Eq. (1)), it can be shown later that

$$|\Delta| << 1. \tag{31}$$

We can find the analytical solutions of Eq. (29) for different regions of k where some approximations can be made on the terms in Eq. (29)

A. Short Wavelength Mode ($k < k_-^b$, $k > k_+^b$)

For $k < k_-^b$ or $k > k_+^b$ (see Fig. 2 and Eqs. (14) and (17)), we have

$$|\Omega_s^2 - \omega_{ln}^2| >> 2\Omega_s |\Delta|,$$
$$|\Omega_s^2 - \omega_{ln}^2| >> |\Delta^2|,$$
$$\beta_\perp^2 H |\Omega_s^2 - k^2| >> 2 |\Delta| \left| \frac{Q}{s} - \beta_\perp^2 H \Omega_s \right|, \tag{32}$$
$$\beta_\perp^2 H |\Omega_s^2 - k^2| >> |\Delta|^2 |U - \beta_\perp^2 H|,$$

so that Eq. (29) can be approximated or

$$\Delta^2 (\Omega_s^2 - \omega_{ln}^2) + \frac{\eta}{R^2} (\Omega_s^2 - k^2) = 0. \tag{33}$$

Here small quantity η is defined in Eq. (25). The solution of the quadratic Eq. (33) is given by

$$\Delta_r = 0,$$
$$\Delta_i = \frac{\eta^{\frac{1}{2}}}{R} \left[\frac{k^2 - \Omega_s^2}{\omega_{ln}^2 - \Omega_s^2} \right]^{1/2} \tag{35}$$

where Δ_r and Δ_i are the real and imaginary parts of Δ, and ω_{ln} and Ω_s are given by Eq. (13). We note that the growth rate Δ_i is proportional to $(\eta)^{\frac{1}{2}}$, that it is a monotonic function of axial wavenumber k, approaching $\eta^{\frac{1}{2}}/R$ as $|k|$ increases to infinity, and that the growth rate is a monotonically decreasing function of the wall location R. These are illustrated in Fig. 4. It can be easily proved that at $k = k_\pm^b$ (see Eqs. (14) and (17)), there exists no instability since the dispersion equation becomes linear.

B. Long Wavelength Mode ($k_-^b > k > k_+^b$).

For $k_-^b > k > k_+^b$, (see Fig. 2, and Eqs. (14) and (17)), we have

$$\Omega_s >> |\Delta|,$$
$$\beta_\perp^2 H (\Omega_s^2 - k^2) >> 2|\Delta| \left| \frac{Q}{s} - \beta_\perp^2 H \Omega_s \right|, \tag{36}$$
$$\beta_\perp^2 H (\Omega_s^2 - k^2) >> |\Delta^2| |U - \beta_\perp^2 H|,$$

so that Eq. (29) can be approximated as

$$\Delta^3 + a\,\Delta^2 + b = 0. \tag{37}$$

Here quantities a and b are defined by

$$a \equiv \frac{\Omega_s^2 - \omega_{in}^2}{2\Omega_s}, \tag{38}$$

$$b \equiv \frac{\eta}{R^2}\,\frac{\Omega_s^2 - k^2}{2\Omega_s}. \tag{39}$$

Note that we deliberately retain Δ^3 term, since the long wavelength mode ($k_-^b > k > k_+^b$) included the k-region where the quantity a vanishes (Eq. (15) and Fig. 2). The cubic Eq. (37) can be formally solved as shown in Appendix B. Namely, the complex solution of Eq. (37) is given by

$$\Delta_r = \frac{1}{2}\,[B_+^{\frac{1}{3}} + B_-^{\frac{1}{3}}], \tag{40}$$

$$\Delta_i = \frac{\sqrt{3}}{2}\,[B_+^{\frac{1}{3}} - B_-^{\frac{1}{3}}], \tag{41}$$

where

$$B_\pm \equiv \frac{b}{2} + \frac{a^3}{27} \pm d, \tag{42}$$

$$d^2 \equiv b\left[\frac{b}{4} + \frac{a^3}{27}\right]. \tag{43}$$

The necessary and sufficient condition for instability (i.e., $\Delta_i > 0$) is readily obtained.

$$d^2 > 0. \tag{44}$$

We note that for the long wavelength mode ($k_-^b > k > k_+^b$),

$$\begin{aligned} b &> 0, \\ B_+ &> B_- \geqslant 0, \\ B_+B_- &= \left(\frac{a}{3}\right)^6. \end{aligned} \tag{45}$$

The growth rate of the long wavelength mode, Eq. (41) will be extensively analyzed in the next two chapters.

We have seen that there exist two branches of the electron cyclotron instabilities. These are identified as the long wavelength and the short wavelength modes. These modes are separated by band of stable region in the axial wavenumber (k) near $k = k_{\pm}^{b}$ (see Fig. 4), and the growth rate of the long wavelength mode, as it turned out later, is in the order of $\eta^{\frac{1}{3}}$ (see Eq. (25)), while that of the short wavelength mode is in the order of $\eta^{\frac{1}{2}}$. At usual parameters (see Eq. (50)), the growth rate of the long wavelength mode is four times higher than that of the short wavelength mode. We also note that the axial group velocity of the waveguide for the long wavelength mode is in the order of the beam axial velocity, while that for the short wavelength is much higher and is in the order of speed of light (c). The combined effects are such that the amplification of the long wavelength mode is much more dominant than that of the short wavelength mode when both are present. It should also be emphasized that, as discussed in the next chapter, there exist parametric optimum conditions that maximize the growth rate of the long wavelength mode, while such conditions does not exist for the short wavelength mode, which makes it difficult to design an efficient experiment utilizing the short wavelength mode. It is, however, possible that for some particular experimental situations the amplification due to the short wavelength mode may be comparable to or even higher than that due to the long wavelength mode. For this reason, we can not completely forsake the study on the short wavelength mode. It is pointed out that there is neither the experimental proof of the existence nor the plausible explanation of the physical mechanism responsible for the short wavelength mode yet.

IV. LONG WAVELENGTH MODES

The long wavelength mode instability is defined as a growing mode whose axial wavenumber is within the range of $k_{-}^{b} < k < k_{+}^{b}$, where $k_{\pm}^{b}$ are defined by Eq. (17). The

growth rate for the long wavelength mode is given by approximate solution (41). Generally the growth rate Δ_l is a function of following normalized parameters.

$$\Delta_l = \Delta_l\,(k,\ R;\ r_0;\ n,\ l,\ s;\ \beta_\perp,\ \beta_z,\ \nu) \tag{46}$$

The various parameters are; the axial wavenumber, the conducting wall radius, the beam center radius, the radial node number, the azimuthal mode number, the magnetic harmonic number, the transverse speed, the axial speed, and the density (Budker parameter). In this chapter we will discuss the behavior of the growth rates with respect to the axial wavenumber (k) and the wall radius (R), while all the rest parameters are assumed to be given. The examinations consist of analysis on properties of quantities appearing in growth rate Eq. (41), the determination of the instability boundary, and maximization of the growth rate in $k - R$ space. We adopt the notation $\hat{}$ as optimum value that maximize the growth rate.

It is our intention to obtain as much information on the general properties and tendencies of the growth rate as possible without actually solving the growth rate Eq. (41). This analytical approach is possible primarily due to the tenuous assumption [see Eq. (1)]. This small density assumption can be expressed as

$$\eta \ll 1, \tag{47}$$

where η is defined by Eq. (25), namely

$$\eta \equiv \frac{2\nu\ \gamma_z^2\ \beta_\perp^2}{\gamma_0 N_{ln}}\ [J_{s-l}\,(X_0)\ J_s'(X_L)]^2. \tag{48}$$

Here $H_{ln}\,(X_o,\ X_L)$ of Eq. (25) is explicitely shown, and quantities X_o, and X_L are given by

$$X_0 \equiv X_{ln}\ r_0, \tag{8}$$

$$X_L \equiv \frac{\gamma_z \beta_\perp}{R}\ s. \tag{13}$$

Using typical experimental parameters given by

$$\nu = 3 \times 10^{-3},\ \beta_\perp = 0.3,\ \beta_z = 0.2, \tag{49}$$
$$s = l = n = 1,\ r_o = 0,\ R = 1,$$

the values of small quantity η and its fractional powers are

$$\eta = 2.7 \times 10^{-4},\ \eta^{\frac{1}{2}} = 1.6 \times 10^{-2}, \tag{50}$$

$$\eta^{\frac{1}{3}} = 6.4 \times 10^{-2},\ \eta^{\frac{1}{6}} = 2.5 \times 10^{-1}.$$

It should be mentioned here that the mode $s = l = n = 1$ with $r_0 = 0$, $R \simeq 1$ yields the highest growth rate in entire (l, n, s) modes. That is to say that, for given ν, $\beta_\perp$ and β_z, the values given in Eq. (50) are their upper limits. The smallness of η enables us to approximate equations so that their graphic solutions and estimations of the numerical values of solutions are frequently possible to obtain.

It is convenient to consider the growth rate Δ_i as a function of the quantities $a(k, R)$ and $b(k, R)$ defined by Eq. (38) and (39) respectively. The quantity a determines the difference between two eigenfrequencies of the system, namely, the Doppler-shifted cyclotron frequency, Ω_s (Eq. (13)) and the free wave guide frequency, ω_{ln} (Eq. (13)); while the quantity b measures the difference in phase velocities between the beam-waveguide eigenmodes and the free electromagnetic wave in vacuum. We will examine the functional dependencies of a and b on k and R for future references. With some algebra, the quantities a and b can be written as

$$a = \frac{1}{2\gamma_z^2}\,\frac{1}{\Omega_s}\,(k_+^a - k)\,(k - k_-^a), \tag{51}$$

$$b = \frac{\eta}{R^2}\,\frac{1}{2\gamma_z^2}\,\frac{1}{\Omega_s}\,(k_+^b - k)\,(k - k_-^b), \tag{52}$$

where $k_\pm^a$ and $k_\pm^b$ are given by Eqs. (18) and (17). If we differentiate a and b with respect to k, it is straightforward to show

$$\frac{\partial a}{\partial k} = \frac{\beta_z}{2\gamma_z^2}\,\frac{1}{\Omega_s^2}\,(k_0^a - k)\,(k + k_\uparrow^a), \tag{53}$$

$$\frac{\partial b}{\partial k} = \frac{\beta_z}{2\gamma_z^2}\,\frac{\eta}{R^2}\,\frac{1}{\Omega_s^2}\,(k_0^b - k)\,(k + k_\uparrow^b), \tag{54}$$

where

$$\begin{Bmatrix} k_o^a \\ k_1^a \end{Bmatrix} \equiv \frac{1}{\beta_z} \left[\gamma_z \left(1 + \gamma_z^2 \beta_z^2 / R^2\right)^{1/2} \mp 1\right], \tag{55}$$

$$\begin{Bmatrix} k_o^b \\ k_1^b \end{Bmatrix} \equiv \frac{1}{\beta_z} \left[\gamma_z \mp 1\right]. \tag{56}$$

The plots of $k_\pm^a$, k_o^a, $k_\pm^b$, and k_o^b in $k - R$ space are given in Fig. 5. We note that $k_o^a > k_o^b$ and that $k_-^b < k_-^a \leqslant k_+^a \leqslant k_+^b$ when $R \geqslant 1$. For $R < 1$, $k_\pm^a$ are not defined. While $k_\pm^a$ and k_o^a are functions of R, the quantities $k_\pm^b$ and k_o^b are independent of R. The Eqs. (51) to (54) indicate that

$$a \underset{<}{>} 0 \text{ when } \begin{Bmatrix} k_+^a > k > k_-^a \\ k > k_+^a \text{ or } k < k_-^a \end{Bmatrix}, \tag{57}$$

$$b > 0 \text{ for } k_+^b > k > k_-^b, \tag{58}$$

$$\frac{\partial a}{\partial k} \underset{<}{>} 0 \text{ when } k \underset{<}{>} k_o^a, \tag{59}$$

and

$$\frac{\partial b}{\partial k} \underset{<}{>} 0 \text{ when } k \underset{>}{<} k_o^b. \tag{60}$$

Note that, from Eq. (58), $b > 0$ for long wavelength modes. For future reference we define the wall radius of the intersection of k_o^b line and k_-^a curve as R_o as shown in Fig. 5, and its magnitude is given by

$$R_o = \left[\frac{\gamma_z + 1}{2}\right]^{1/2}. \tag{61}$$

With $\beta_z = 0.2$, $R_o = 1.005$. The wall radius (R) dependences of a and b can be shown as (Appendix C)

$$\frac{\partial a}{\partial R} = \gamma_z^2 \frac{1}{\Omega_s R^3}, \tag{62}$$

$$\frac{\partial b}{\partial R} = -\eta \frac{(\Omega_s^2 - k^2)}{\Omega_s R^3} \frac{(s^2 - X_L^2)}{X_L} \frac{J_s(X_L)}{J_s'(X_L)}. \tag{63}$$

The determination of the sign of $\partial b/\partial R$ is complicated since the sign depends on the signs of the terms, $(s^2 - X_L^2)$, $J_s(X_L)$ and $J_s'(X_L)$. It can be shown, however, that

$$\frac{\partial b}{\partial R} < 0 \text{ when } R > \gamma_z \beta_\perp \tag{64}$$

as shown in Appendix C. It should be noted that the condition $R > \gamma_z \beta_\perp$ is easily satisfied for weakly relativistic ($\gamma_o \sim 1$) beam electrons as in usual gyrotron devices. The derivatives of the quantities a and b with respect to the wavenumber k and the wall radius R (i.e., Eqs. (53), (54), (62), and (63)) are computed for the purpose of finding the location of the maximum growth rate in $k - R$ space later.

A. Instability Boundary

Before discussing the magnitudes of the growth rates, it is instructive to examine the instability criteria. This will determine the instability boundary in $k - R$ space, and thereby the instability area, which is closely related to the bandwidth and the cut-off value of the wall radius, which is important in designing gyrotron devices.

The necessary and sufficient condition for the long wavelength instability is given by Eq. (44) (see Appendix B), which can be written as

$$\frac{a^3}{27} > -\frac{b}{4}. \tag{65}$$

The quantities a and b are given by Eqs. (51) and (52). We again emphasize that b is positive but small (proportional to η) for the long wavelength modes. We realize that solving Eq. (65) is equivalent to solving the growth rate Eq. (41), and resolve to graphic solution of Eq. (65) avoiding much of algebra. The solution of the stability boundary Eq. (65) is graphically illustrated in Fig. 6. The plots of $(a^3/27)$ and $(-b/4)$ versus the wavenumber k are given for several values of the wall radii R designated as I to V. The numerical values of R decreases as the notation changes from I to V, such that $R_I > R_{II} > R_{III} = 1 > R_{IV} > R_V$. The instability region in k is bordered by two intersecting points of $(-b/4)$ and $(a^3/27)$ curves for each R. Since the curve of $(a^3/27)$ at given R nests all $(a^3/27)$ curves at smaller wall radii (see Eq.

(51)) inside, and $(-b/4)$ is a weak function of R (the coefficient is small number η, see Eq. (52)), we conclude that the instability range $\Delta k(R)$ is a montonically increasing function of R, namely

$$\Delta k\ (R_1) > \Delta k(R_2) \text{ if } R_1 > R_2, \tag{66}$$

and that there exists a cutoff wall radius R_B such that

$$\Delta_i\ (R < R_B) = 0. \tag{67}$$

These features are apparent from Fig. 6. The distance between two intersecting points (i.e., Δk) becomes smaller as I goes to V (i.e., as R decreases), and for small R (e.g., R_V) the two curves do not intersect, corresponding no instability. The schematic graph of the stability boundary, denoted as k_B, in $k - R$ space is drawn in Fig. 7. The instability occurs only to the right of the boundary curve k_B, and we note that k_B intersects with k_o^a at R_B, the cutoff wall radius, since $(a^3/27)$ is maximum at k_o^a (see Eq. (53)).

The smallness of η provides information on the location of the boundary curve k_B in $k-R$ space. The boundary k_B is defined by the marginal equation

$$\frac{a^3}{27} = -\frac{b}{4}. \tag{68}$$

Since the quantity b is proportional to small quantity η (Eq. (52)), we expect that the quantity a along k_B is also small and negative. This indicates that the boundary k_B is to the left of $k_\pm^a$ (along which $a = 0$) and is close to $k_\pm^a$ (see Eq. (51)). The distance between k_B and $k_\pm^a$ can be estimated with the teneous beam assumption (viz. smallness of η). With some algebra, it can be shown that

$$|k_B - k_\pm^a| \simeq \begin{cases} \dfrac{1}{\sqrt{3}}\,\gamma_z^2\,\eta^{\frac{1}{6}} & \text{at } R = 1 \\ \dfrac{3}{2}\,\gamma_z^2\,\eta^{\frac{1}{3}}\left[\dfrac{\{1 \pm \beta_z\,(1-1/R^2)^{1/2}\}^2}{R^+\,(1-1/R^2)^{3/2}}\right]^{1/3}, & \text{at } R >> 1 \end{cases} \tag{69}$$

and

$$R_B \simeq 1 - \frac{3}{2}\,\eta^{1/3}. \tag{70}$$

With parameters given by Eqs. (49) and (50), the cutoff wall radius R_B is found to be ~0.904.

The bandwidth of the gyrotron, if we define it by the range of the axial wavenumber k where the instability exists, is given by Eq. (69). With this unconventional definition, the bandwidth increases as the wall radius R increases (see Fig. 6). If, however, the bandwidth is defined by k range where the growth rate falls off to a prescribed fraction of its maximum value, as is conventional, it will be much different from that given by Eq. (69). This is due to the fact that the maximum growth rate in the wavenumber k is a decreasing function of the wall radius R, as will be shown later, thereby making the conventional bandwidth a complicate function of R.

B. Maximization of Growth Rate

In this section we will find the dependence of the growth rate (Δ_i) on the wavenumber k and the wall radius R. Specifically we will examine the signs of $\partial\Delta_i/\partial k$ and $\partial\Delta_i/\partial R$ in $k - R$ space, and find the position where Δ_i is absolute maximum. This will lead to the matching condition on the wall radius R and to the expression for estimated magnitude of the absolute maximum growth rate.

If we differentiate the growth rate equation (41) with respect to k and R, we obtain

$$\frac{\partial\Delta_i}{\partial k} = \frac{\partial b}{\partial k}\,\alpha^2 - a\,\frac{\partial a}{\partial k}\,\beta^2, \tag{71}$$

$$\frac{\partial\Delta_i}{\partial R} = \frac{\partial b}{\partial R}\,\alpha^2 - a\,\frac{\partial a}{\partial R}\,\beta^2, \tag{72}$$

where the coefficients α^2 and β^2 are given by

$$\alpha^2 \equiv \frac{1}{4\sqrt{3}} \frac{1}{d} (B_+^{\frac{1}{3}} + B_-^{\frac{1}{3}}) > 0,$$
$$\beta^2 \equiv \frac{1}{6\sqrt{3}} \frac{1}{d} (B_+^{\frac{1}{6}} - B_-^{\frac{1}{6}}) (B_+^{\frac{1}{3}} - B_-^{\frac{1}{3}}) \geq 0. \tag{73}$$

In Eq. (73) we made use of $B_+ \geq B_-$ (Eq. (45)), and the quantities d and $B_\pm$ are defined by Eqs. (42) and (43). The derivatives, $\partial a/\partial k$, $\partial b/\partial k$, $\partial a/\partial R$, and $\partial b/\partial R$ are given in Eqs. (53), (54), (62), and (64). The curves along which $\partial \Delta_i/\partial k = 0$ are defined by

$$\frac{\partial b}{\partial k} \alpha^2 = a \frac{\partial a}{\partial k} \beta^2, \tag{74}$$

whose schematic solutions are illustrated in Fig. 8. Detailed discussions on these curves are given in Appendix D. As is shown in Fig. 8, there are two branches of $\partial \Delta_i/\partial k = 0$ separated by k_o^a curve. The k-dependence of Δ_i at two representative values of R are also shown in Fig. 8. The lower $\partial \Delta_i/\partial k = 0$ curve, which gives higher maximum growth than that for upper curve, intersects with the stability boundary k_B and with k_-^a curve at the same k_o^b. As discussed in Appendix D, the distance between the lower k-maximum curve and k_o^b line for $R < R_o$ (i.e., to the left of k_-^a curve in Fig. 8) ϵ_k is given by

$$\epsilon_k \sim \eta^{2\delta - 1} \text{ when } \epsilon_R \sim \eta^\delta, \tag{75}$$

where $\epsilon_R \equiv |R - R_o|$. Note that $\delta > \frac{1}{3}$, since for the stability curves k_B, $\epsilon_R \sim \eta^{1/3}$ (Eq. (70)). Similarly, we can find graphic solution for $\partial \Delta_i/\partial R = 0$ defined by

$$\frac{\partial b}{\partial R} \alpha^2 = a \frac{\partial a}{\partial R} \beta^2, \tag{76}$$

and the result is shown in Fig. 9. See Appendix D for more details on this solution. The R-maximum curve ($\partial \Delta_i/\partial R = 0$) lies to the left of the $k_\pm^a$ curve, and its wall radius distance from $k_\pm^a$, ϵ_R is given by

$$\epsilon_R \sim \eta. \tag{77}$$

In Fig. 10, the complete $k-$, $R-$ dependence of Δ_i is shown. Note that $\partial\Delta_i/\partial R = 0$ curve intersect with the lower $\partial\Delta_i/\partial k = 0$ curve, and its intersection coordinates $(\hat{R}, \hat{k})$, where the growth rate is the absolute maximum, are given by (from Eqs. (75) and (77))

$$R_o - \hat{R} \sim \eta, \tag{78}$$

$$\hat{k} - k_o \sim \eta, \tag{79}$$

where the expressions for R_o and k_o^b appear in Eqs. (61) and (56) respectively. In view of smallness of η (Eq. (50)), for practical purpose, we can conclude that the absolute maximum growth exists at

$$\hat{R} \simeq R_o = \left[\frac{\gamma_z + 1}{2}\right]^{1/2} \tag{80}$$

$$\hat{k} \simeq k_o^b = \frac{1}{\beta_z}(\gamma_z - 1) \tag{81}$$

The corresponding real eigenfrequency ω_r is then

$$\hat{\omega}_r \simeq \gamma_z. \tag{82}$$

The growth rate at $R = R_o$ and $k = k_o^b$ can be shown as (see Appendix E)

$$\hat{\Delta}_i = \frac{\sqrt{3}}{2}\left[\frac{2\nu}{\gamma_o N_{lm}} \frac{\gamma_z}{(\gamma_z + 1)}\left\{\frac{\hat{X}_L}{s} J_{s-l}(X_o) J_s'(\hat{X}_L)\right\}^2\right]^{1/3} \tag{83}$$

where the explicite expression for η at R_o is shown , and the quantity $\hat{X}_L$ is defined by

$$\hat{X}_L \equiv s\left[\frac{2\beta_\perp^2 \gamma_z^2}{\gamma_{s+1}}\right]^{1/2}, \tag{84}$$

which is X_L (Eq. (13)) at $R = R_o$.

In summary, we have optimized the growth rates of the long wavelength modes with respect to the wall radius R and the axial wavenumber k for given parameters $(n, l, s, \beta_\perp, \beta_z, \nu)$. The analysis has resulted in the wall radius and the wavenumber matching conditions (Eqs. (80) and (81)), under which the instability gives highest growth rate, and it has been successful in obtaining approximate magnitude of the growth rate. In unnormalized quantities (Eq. (10)), these results are as follow.

$$\hat{R}^{\text{real}} \simeq \left[\frac{\gamma_z + 1}{2\gamma_z^2}\right]^{1/2} \frac{cX_{ln}}{s\omega_c/\gamma_o}, \tag{85}$$

$$\hat{k}^{\text{real}} \simeq \frac{(\gamma_z - 1)}{\beta_z} \frac{s\omega_c/\gamma_o}{c}, \tag{86}$$

$$\hat{\omega}_r^{\text{real}} \simeq s\gamma_z\, \omega_c/\gamma_o, \tag{87}$$

$$\hat{\Delta}_i^{\text{real}} \simeq \frac{\sqrt{3}}{2} s\omega_c/\gamma_o \times \left[\frac{2\nu}{\gamma_o N_{ln}} \frac{\gamma_z}{(\gamma_z + 1)} \left\{\frac{\hat{X}_L}{s} J_{s-l}(X_o)\, J_s'(\hat{X}_L)\right\}^2\right]^{1/3}. \tag{88}$$

We add here that the matching conditions (85), and (86), and their results (87), and (88) are still valid for coaxial gyrotrons if appropriate combined Bessel functions and their zeros are replaced in Eqs. (85) and (88). It is not repetitive to emphasize that the possibility of obtaining these approximate results rest on the tenuous density ($\nu << 1$, or $\eta << 1$) assumption.

V. PARAMETRIC OPTIMIZATION OF GROWTH RATE

In previous chapter we have maximized the growth rate of the long wavelength mode with respect to the wall radius R and the axial wavenumber k while the rest parameters are assumed to be given. In this chapter we further optimize the growth rate with respect to the beam center location r_o, (section A) the radial node number n (section B), and the azimuthal mode number l (section C) in that order. For each step of optimization we start with the growth rate already optimized with respect to all previous parameters unless stated otherwise. In final section (D) we will discuss the dependence of the growth rate on the magnetic harmonic number s. Again we adopt the notation $\hat{}$ as optimum value.

A. Beam Center Optimization (r_o)

For given ν, $\beta_\perp$ β_z, s, l and n, the k and R optimized growth rate is given by Eq. (83). The only part in Eq. (83) that is dependent of the beam center location r_o is $J_{s-l}(X_o)$ term through $X_0 \equiv X_{ln}\, r_o$. Namely,

$$\Delta_l \propto [J_{s-l}(X_0)]^{2/3}, \tag{89}$$

where

$$X_0 \equiv X_{ln}\, r_o. \tag{8}$$

Before optimization of $J_{s-l}(X_o)$ with respect to r_o (X_o), we recognize that there exist a physical constraint in X_o variation. By insisting that the beam must lie within the conductor, that is, in unnormalized real values,

$$r_o^{\text{real}} + r_L^{\text{real}} \leqslant R^{\text{real}}, \tag{90}$$

which can be expressed with normalized variables as

$$X_o \leqslant X_{ln} - X_L. \tag{91}$$

From properties of Bessel functions, we can show that

$$1 > |J_{s-l}(X_{|s-l|1})| > |J_{s-l}(X)|, \quad \text{if } s \neq l, \text{ and } X \neq X_{|s-l|1} \tag{92}$$

and

$$1 = |J_o(0)| > |J_o(X)| \text{ if } X > 0. \tag{93}$$

Here $X_{|s-l|1}$ is the first positive zero of $J'_{s-l}(x)$ when $s - l \neq 0$. It is evident that the maximum value of $|J_{s-l}(X_o)|$ depends on $(s - l)$, and when $s \neq l$ on the magnitudes of X_o and $X_{|s-l|1}$. We conclude that

$$|J_{s-l}(X_o)|_{\max} = J_{sl}^o \tag{94}$$

where

$$J_{sl}^o \equiv \begin{cases} 1 \text{ if } s = l, & \text{(95-a)} \\ |J_{s-l}(X_{|s-l|1})| \quad \text{if } s \neq l,\ X_{ln} - X_L \geqslant X_{|s-l|1}, & \text{(95-b)} \\ |J_{s-l}(X_{ln} - X_L)| \quad \text{if } s \neq l,\ X_{ln} - X_L < X_{|s-l|1}, & \text{(95-c)} \end{cases}$$

and the corresponding optimum beam center location $\hat{r}_o$ is given by

$$\hat{r}_o = \begin{cases} 0 \qquad \text{if } s = l, & \text{(96-a)} \\ \dfrac{X_{|s-l|1}}{X_{ln}} \qquad \text{if } s \neq l,\ X_{ln} - X_L \geqslant X_{|s-l|1}, & \text{(96-b)} \\ \dfrac{X_{ln} - X_L}{X_{ln}} \qquad \text{if } s \neq l,\ X_{ln} - X_L < X_{|s-l|1}. & \text{(96-c)} \end{cases}$$

Note that

$$J^o_{sl}\,(95\text{-}a) > J^o_{sl}\,(95\text{-}b) > J^o_{s-l}\,(95\text{-}c). \tag{97}$$

In this regards the process of r_o optimization is in part that of optimization of the azimuthal mode number l for given magnetic harmonic number s. With r_o optimization given by Eqs. (94) to (96), the maximum growth rate $\hat{\Delta}_i$ becomes,

$$\hat{\Delta}_i = \frac{\sqrt{3}}{2}\left[\frac{2\nu}{\gamma_o N_{ln}}\,\frac{\gamma_z}{(\gamma_z+1)}\left\{\frac{\hat{X}_L}{s}\,J^o_{sl}\,J_s'\,(\hat{X}_L)\right\}^2\right]^{1/3}. \tag{98}$$

We mention here that the optimized beam center location (i.e., $s = l$, $r_0 = 0$) corresponds to so called "rotating beam", which is quite different from usual gyrotron gun, and is best produced by cusp magnetic fields such as Maryland ERA machine. We also add here that when the beam center optimization is not realized to its potential as the case is for Eq. (95-c), there will be competition between the wall radius optimization (Eq. (80)), and r_o optimization via wall radius variation. This kind of competition is present in almost every step of optimization, for which more careful study is in need. It is important to point out that for $s = l$ device, this $R - r_o$ competition is absent.

B. Radial Node Optimization (n)

The dependence of the growth rate on the radial node number (n), after r_o optimization, is given by

$$\Delta_i \propto \left(\frac{1}{N_{ln}}\right)^{1/3}. \tag{99}$$

The term N_{ln} originally appeared in the dispersion equation from orthogonal integration of Bessel function, that is,

$$N_{ln} \equiv \int_o^{X_{ln}} X dX\; J_l^2(X). \tag{100}$$

Since X_{ln} is an increasing function of $|l|$ and n, it is obvious that N_{ln} is also an increasing function of $|l|$ and n. Therefore we conclude that the growth rate Δ_i is a decreasing function of the radial node number n. Caution must be taken here about the competition between n and r_o optimizations. As n decreases, so does X_{ln}, thereby raising possibility for violation of full optimization of beam center location (Eq. (95-c)). This competition is absent again for $s = l$ device.

C. Azimuthal Mode Optimization (l)

The dependence of the growth rate on the azimuthal mode number (l) for given magnetic harmonic number s is given by

$$\Delta_i \propto \left[\frac{1}{N_{ln}} \left\{J_{sl}^o\right\}^2\right]^{1/3} \tag{101}$$

after the beam center radius (r_o) optimization (Eq. (98)). Obviously Δ_i is a function of both s and l, and the combination makes it difficult to conclude on l dependence in simplicistic way. However, since $J_{sl}^o = J_{s-l}\,(X_{|s-l|1})$ is rapidly decreasing near $l = s$, we expect that Δ_i will be maximum when $l = s$, unless the magnetic number s is extremely high. If we ignore the full optimization rule restriction on beam center radius (Eq. (95-b)), the quantity $\left[\frac{1}{N_{ln}} \{J_{sl}^o\}^2\right]^{1/3}$ is completely independent of other parameters and their numerical values are easily calculated. Fig. 11 gives the plot of the quantity $\left[\frac{1}{N_{ln}} J_{sl}^{o2}\right]^{1/3}$ versus the azimuthal mode number l for $s = 1$ to 4. The values are not to be compared for different s, since the quantity has not included other dependences. However for given s, these values are proportional to their growth rates (Eq. (101)), so that the magnitudes for different l can be directly compared. At this low magnetic number, it is obvious that $s = l$ growth rate is much higher than that for $s \neq l$. The points with cross marks indicate the violation of the beam center radius optimization.

That is, for the azimuthal wavenumber l with crossed points, the growth rates are less than those shown in Fig. 11. The graph also reveals that except for $s = 1$, the next highest growth rate is for the mode with $l = s - 1$. When $s = 1$, the growth rate for $l = 0$ is less than that for $l = 2$. The comparison of TE_{s1s} with TE_{01s} (azimuthally symmetric $l = 0$ mode) shows that

$$\Delta_i (TE_{s1s}) = 2 \times \Delta_i (TE_{01s}), \tag{102}$$

where TE_{lns} notations are used. The optimization rule becomes then

$$\hat{l}_1 = s. \tag{103}$$

with

$$\begin{aligned} \hat{l}_2 &= s - 1 \quad \text{if } s > 1, \\ \hat{l}_2 &= 0 \quad \text{if } s = 1, \end{aligned} \tag{104}$$

as next optimum value. With $l = s$ mode, the growth rate becomes

$$\hat{\Delta}_i = \frac{\sqrt{3}}{2} \left[\frac{2\nu}{\gamma_o N_{ln}} \frac{\gamma_z}{(\gamma_z + 1)} \left\{ \frac{\hat{X}_L}{s} J'_s (\hat{X}_L) \right\}^2 \right]^{1/3}. \tag{105}$$

The corresponding beam center location is

$$\hat{r}_o = 0. \tag{106}$$

D. Harmonic Number (s) Dependence

The growth rate, optimized on wavenumber ($\hat{k} \simeq k_o^b$), wall radius ($\hat{R} \simeq R_o$), beam center at radius ($\hat{r}_o = o$), and azimuthal mode number ($\hat{l} = s$) depends on the magnetic harmonic number (s) according to (Eq. (105))

$$\hat{\Delta}_i \alpha \left[\frac{1}{N_{ln}} \frac{\hat{X}_L^2}{s^2} \{ J'_s (\hat{X}_L) \}^2 \right]^{1/3}, \tag{107}$$

where the argument of Bessel function $\hat{X}_l$ is defined by

$$\hat{X}_L \equiv \left[\frac{2\beta_\perp^2 \gamma_z^2}{(\gamma_z + 1)} \right]^{1/2} s. \tag{24}$$

It is obvious from Eq. (84) that general properties of Δ_i on s are difficult to obtain. It is, however, possible to get an approximated expression for $J_s'(\hat{X}_L)$ at certain conditions. As shown in Appendix F, if

$$s \frac{\beta_\perp^2 \gamma_z^2}{(\gamma_z + 1)} << 2, \tag{108}$$

then

$$J_s'(\hat{X}_L) \simeq \frac{1}{2} \left[\frac{e\beta_\perp \gamma_z}{\{2(\gamma_z + 1)\}^{1/2}} \right]^{s-1}. \tag{109}$$

where e is the base of natural logarithms ($e = 2.71828$). The condition (108) can be considered as limits both on the relativistic factor of beam electrons ($\beta_\perp$, γ_z) and on the magnetic harmonic number s for the validity of approximate expression (109). We mention here that, for usual gyrotrons, the relativistic factor is so low that expression (109) is valid for all the range of magnetic number s in interest. When the Eq. (108) is satisfied, it is easy to show with (109) that

$$\frac{\hat{X}_L^2}{s^2} \{J_s'(\hat{X}_L)\}^2 \geq \frac{2}{e^2} \left[\frac{e^2 \beta_\perp^2 \gamma_z^2}{2(\gamma_z + 1)} \right]^s. \tag{110}$$

The other s-dependent term in Δ_i (Eq. (107)), namely, $1/N_{sn}$ is a decreasing function of s, but as can be seen from Fig. 11, it is a weak function of s, compared with s-dependence of Eq. (110). We can therefore conclude that

$$\hat{\Delta}_i(s) \mid \left[\frac{e^2 \beta_\perp^2 \gamma_z^2}{2(\gamma_z + 1)} \right]^{s/3}, \tag{111}$$

or

$$\hat{\Delta}_i(s) = \hat{\Delta}_i(s-1) \left[\frac{e^2 \beta_\perp^2 \gamma_z^2}{2(\gamma_z + 1)} \right]^{\frac{s-1}{3}}. \tag{112}$$

If the relativistic factor is low such that

$$\frac{\beta_\perp \gamma_z^2}{\gamma_z + 1} < \frac{2}{e^2}, \tag{113}$$

then the growth rate Eq. (112) is a monotonically decreasing function of s. Usual gyrotron devices easily satisfy the condition (113). The dependence of the growth rate of $s = l$ mode on s is illustrated in Fig. 12.

If we combine all the optimizing processes, we obtain the highest maximum growth rate, which is given by

$$\hat{\Delta}_i^{\max} = \frac{\sqrt{3}}{2}\left[\frac{2\nu}{\gamma_o N_{11}}\,\frac{\beta_\perp^2\,\gamma_z^3}{(\gamma_z+1)^2}\right]^{1/3}. \tag{114}$$

The highest growth rate of Eq. (114) is obtained with the following optimizations.

$$\hat{k} \simeq k_o^b = \frac{1}{\beta_z}(\gamma_z - 1) \tag{81}$$

$$\hat{R} \simeq R_o = \left[\frac{\gamma_z+1}{2}\right]^{1/2} \tag{80}$$

$$\hat{r}_o = 0 \tag{96-a}$$

$$\hat{l} = \hat{n} = \hat{s} = 1 \tag{103,111}$$

In unnormalized quantities, the highest growth rate is for TE_{111} ($l = 1$, $n = 1$, $s = 1$) mode with

$$\hat{R}^{\text{real}} \simeq \left[\frac{\gamma_z+1}{2\gamma_z^2}\right]^{1/2}\frac{cX_{11}}{s\omega_c/\gamma_o}, \tag{115}$$

$$\hat{k}^{\text{real}} \simeq \left[\frac{\gamma_z-1}{\beta_z}\right]\frac{s\omega_c/\gamma_o}{c}, \tag{116}$$

$$\hat{r}_o^{\text{real}} = 0, \tag{117}$$

$$\hat{\omega}_r^{\text{real}} = s\,\gamma_z\,\omega_c/\gamma_o, \tag{118}$$

$$\hat{\Delta}_i^{\text{real}} = \frac{\sqrt{3}}{2}\,s\omega_c/\gamma_o\left[\frac{2\nu}{\gamma_o N_{11}}\,\frac{\beta_\perp\,\delta_z^3}{(\gamma_z+1)^2}\right]^{1/3}. \tag{119}$$

We note that $\hat{\Delta}_i^{\max}$ (Eq. (114)) is a monotonically decreasing function of γ_z for given γ_o. That is, for given total particle energy, the growth rate is highest when the electron has no axial speed.

So far we have considered the parametric optimizations of the long wavelength modes. This processes have been equivalent to maximizing $\eta^{1/3}$ (Eq. (48)). We note that the growth

rate for the short wavelength (see chapt. III) is proportional to $\eta^{1/2}$, and conclude that the above procedures will apply the same way to the short wavelength modes as well except for the exponent (1/2) instead of (1/3) for the long wavelength modes. It should be emphasized that while the long wavelength mode possesses optimum wavenumber and wall radius, the short wavelength growth rate increases as $|k|$ increases and as R decreases.

VI. CONCLUSIONS

We have examined the linearized growth rates for TE_{lns} modes of the electron cyclotron maser instabilities with zero-temperature beam electrons. We have found (chapt. III) that there exist two different types of instability modes distinguished by their wavelengths; the short wavelength mode and the long wavelength mode. Assuming that the electron beam is tenuous, we have been able to obtain approximate expressions for the growth rates for both types of modes (Eqs. (35) and (41)), and found that the growth rate for the long wavelength mode is much higher than that for the short wavelength mode at usual parameter range. We have also found that while the long wavelength mode has optimum axial wavenumber and wall radius that maximizes the growth rate, the short wavelength mode does not (see Fig. 4).

We then have maximized the growth rate of the long wavelength mode with respect to various parameters, and have found the optimizing conditions on the parameters. These results are given in Table I.

The growth rate is found to be scaled with the harmonic number s accoridng to Eq. (112), namely

$$\Delta_i(s) = \Delta_i(s=1)\left[\frac{e^2\beta_\perp^2\gamma_z^2}{2(\gamma_z+1)}\right]^{\frac{s-1}{3}}$$

when the beam electrons are weakly relativistic.

We add finally that some of foregoing optimization processes may compete with the other optimizations, and a compromise between them may result in. One example of these situations is given in the text following Eq. (98). Whenever this competition rises, the original growth rate equation (41) should be referred to. The numerical calculations of the growth rates have been carried out and those results will be reported elsewhere.

Acknowledgments

One of the authors (JYC) was supported in part by the Department of Energy for this work.

Appendix A. Roots near Local Extrema

In this appendix, we examine the roots of $f(x) = 0$ near local extremum x_o, where $f'(x_o) = 0$. If $f(x)$ is Taylor expanded near x_o, then

$$f(\epsilon) = f_o + \frac{1}{2} f_o'' \epsilon^2 + \frac{1}{6} f_o''' \epsilon^3 + \cdots, \tag{A-1}$$

where

$$\epsilon \equiv x - x_o, \tag{A-2}$$

$$f_o^{(n)} \equiv \frac{d^n}{dx^n} f(x)|_{x = x_o}$$

In case when

$$|f_o''| >> |\epsilon|\,|f_o'''|, \tag{A-3}$$

the equation $f(\epsilon)=0$ can be approximated as a quadratic equation. Namely,

$$f(\epsilon) = f_o + \frac{1}{2} f_o'' \epsilon^2 = 0, \tag{A-4}$$

whose solution are given by

$$\epsilon = \pm i\Delta, \text{ if } \Delta^2 > 0, \tag{A-5a}$$

$$\epsilon = \pm|\Delta|, \text{ if } \Delta^2 < 0. \tag{A-5b}$$

Here Δ^2 is defined by

$$\Delta^2 \equiv \frac{2f_o}{f_o''}. \tag{A-6}$$

With Eq. (A-5), the validity of Eq. (A-4) (i.e. condition (A-3)) can be written as

$$|f_o''|^3 >> |f_o|\,|f_o'''|^2. \tag{A-7}$$

In summarization, when x_0 is a local extremum of function $f(x)$, viz $f'(x_o) = 0$, the roots of the equation $f(x) = 0$ are given by

$$x = x_o \pm i\left|\frac{f_o''}{f_o'''}\right|^{\frac{1}{2}}, \tag{A-8a}$$

if

$$0 < \frac{f_o}{f_o''} << \left|\frac{f_o''}{f_o'''}\right|^2, \tag{A-9a}$$

and by

$$x = x_o \pm \left[-\frac{2f_o}{f_o''}\right]^{\frac{1}{2}}, \tag{A-8b}$$

if

$$-\left|\frac{f_o''}{f_o'''}\right|^2 << \frac{f_o}{f_o''} < 0. \tag{A-9b}$$

Notice that $f(x) = 0$ have complex roots when f_o and f_o'' have same signs (Eq. 9a).

When the condition (A-7) is not satisfied, the quadratic approximation Eq. (A-4) is no longer possible, and we have to resolve to the cubic or further equation to find the roots. The condition (A-7) can be violated when $|f_o''|$ is too small and/or $|f_o|$ is too large. That is, in order to have complex roots, the equation $f(x)$ must have small $|f_o|$ large $|f_o''|$ in addition to same sign of f_o and f_o''.

Appendix B. Roots of Cubic Equation

We will summarize the properties of roots of the cubic equation given by

$$x^3 + \alpha x^2 + \beta x + \gamma = 0, \tag{B-1}$$

where α, β, and γ are real. With substitution of

$$y \equiv x + \frac{\alpha}{3}, \tag{B-2}$$

Eq. (B-1) becomes

$$y^3 + 3py + q = 0, \tag{B-3}$$

where

$$p \equiv \frac{1}{q}\,[3\beta - \alpha^2],$$
$$q \equiv \frac{1}{27}\,[2\alpha^3 - 9\alpha\beta + 27\gamma]. \tag{B-4}$$

The roots of Eq. (B-3) are found to be

$$y = \begin{Bmatrix} A^{\frac{1}{3}} + B^{\frac{1}{3}} \\ -\frac{1}{2}\,A^{\frac{1}{3}} \pm i\,\frac{\sqrt{3}}{2}\,B^{\frac{1}{3}} \end{Bmatrix}, \tag{B-5}$$

where

$$\begin{Bmatrix} A \\ B \end{Bmatrix} = \frac{1}{2}\,[q \pm (d^2)^{\frac{1}{2}}]. \tag{B-6}$$

Here the determinant d^2 is defined by

$$d^2 \equiv q^2 + 4p^3. \tag{B-7}$$

Note that the necessary and sufficient condition for Eq. (B-1) to have complex roots is given by

$$d^2 > 0. \tag{B-8}$$

Appendix C. Derivations of Equation (62)-(64)

The functions $a(R)$ and $b(R)$ are given by

$$a \equiv \frac{\Omega_s^2 - \omega_{ln}^2}{2\Omega_s}, \tag{38}$$

$$b \equiv \frac{\eta}{R^2} \frac{\Omega_s^2 - k^2}{2\Omega_s}, \tag{39}$$

where

$$\Omega_s \equiv k\beta_z + 1, \tag{6}$$

$$\omega_{ln}^2 = k^2 + \frac{\gamma_z^2}{R^2},$$

and

$$\eta \equiv \frac{2\nu\, \gamma_z^2\, \beta_\perp^2}{\gamma_o N_{ln}} [J_{s-l}(X_o)\, J_s'(X_L)]^2. \tag{48}$$

Here ν, γ_z, $\beta_\perp$, γ_o, N_{ln}, X_o and Ω_s are independent of R, and X_L is

$$X_L \equiv \frac{\gamma_z \beta_\perp}{R} s. \tag{13}$$

We will find the expressions for $\partial a/\partial R$ (62) and $\partial b/\partial R$ (63). If we differentiate Eq. (38) with respect to R, we get

$$\frac{\partial a}{\partial R} = -\frac{1}{2\Omega s} \frac{\partial}{\partial R} (\omega_{ln}^2)$$

$$= \gamma_z^2 \frac{1}{\Omega_s R^3}. \tag{62}$$

Similarly, for b, we have

$$\frac{\partial b}{\partial R} = \frac{(\Omega_s^2 - k^2)}{2\Omega_s} \left[-\frac{2\eta}{R^3} + \frac{1}{R} \frac{\partial \eta}{\partial R} \right]. \tag{C-1}$$

We note that, from Eqs. (48) and (13),

$$\frac{\partial \eta}{\partial R} = 2\eta \frac{J_s''(X_L)}{J_s'(X_L)} \frac{\partial X_L}{\partial R}$$

$$= -\frac{2\eta}{R} \frac{J_s''(X_L)}{J_s'(X_L)} X_L. \tag{C-2}$$

By making use of Bessel identity,

$$X_L J_s''(X_L) + J_s'(X_L) + \frac{X_L^2 - s^2}{X_L} J_s(X_L) = 0, \tag{C-3}$$

the equation (C-2) becomes

$$\frac{\partial \eta}{\partial R} = \frac{2\eta}{R}\left[1 - \frac{s^2 - X_L^2}{X_L}\frac{J_s(X_L)}{J_s'(X_L)}\right]. \tag{C-4}$$

With substitution of Eq. (C-4), Eq. (C-1) is now

$$\frac{\partial b}{\partial R} = \Gamma \eta \frac{(\Omega_s^2 - k^2)}{\Omega_s R^3}\frac{(s^2 - X_L^2)}{X_L}\frac{J_s(X_L)}{J_s'(X_L)}. \tag{63}$$

For derivation of Eq. (64), we first note that for long wavelength modes (i.e. $k_-^b < k < k_+^b$) the term $(\Omega_s^2 - k^2)$, in Eq. (63) is positive. When

$$R > \gamma_z \beta_\perp \tag{C-5}$$

we have from Eq. (13) above

$$X_L < s. \tag{C-6}$$

If we denote the first zero of $J_s'(X)$ for $s \geq 1$ as X_{s1} (> 0), namely, $J_s'(X_{s1}) = 0$, then from Eq. (C-3)

$$X_{s1}^2 - s^2 = -X_{s1}^2 \frac{J_s''(X_{s1})}{J_s(X_{s1})}. \tag{C-7}$$

The fact that J_s has its first maximum at X_{s1} (i.e. $J'_s(X_{s1}) = 0$) indicates that

$$J_s(X_{s1}) > 0,\ J_s''(X_{s2}) < 0. \tag{C-8}$$

With Eq. (C-8), the Eq. (C-7) becomes

$$X_{s1} > s. \tag{C-9}$$

By combining Eqs. (C-5) and (C-1), we obtain

$$X_L < s < X_{s1}. \tag{C-10}$$

Therefore we can easily show that

$$\begin{aligned} J_s(X_L) &> 0, \\ J_s'(X_L) &> 0, \end{aligned} \tag{C-11}$$

if the condition (C-5) is satisfied. From Eqs. (63), and (C-11), it is proven that

$$\frac{\partial b}{\partial R} < 0 \text{ when } R > \gamma_z \beta_\perp. \tag{65}$$

Appendix D. $\partial\Delta_i/\partial k = 0$ and $\partial\Delta_i/\partial R = 0$ Curves.

The curves along which $\partial\Delta_i/\partial k = 0$ are defined by

$$\frac{\partial b}{\partial k}\,\alpha^2 = a\,\frac{\partial a}{\partial k}\,\beta^2, \tag{74}$$

where

$$\frac{\partial a}{\partial k} = \frac{\beta_z}{2\gamma_z^2}\,\frac{1}{\Omega_s^2}\,(k_o^a - k)\,(k + k_1^a), \tag{53}$$

$$\frac{\partial b}{\partial k} = \frac{\beta z}{2\gamma_z^L}\,\frac{\eta}{R^2}\,\frac{1}{\Omega_x^2}\,(k_o^b - k)\,(k + k_1^b), \tag{54}$$

and

$$\alpha^2 = \frac{1}{4\sqrt{3}}\,\frac{1}{d}\,(B_+^{\frac{1}{3}} + B_-^{\frac{1}{3}}) > 0$$

$$\beta^2 = \frac{1}{6\sqrt{3}}\,\frac{1}{d}\,(B_+^{\frac{1}{6}} - B_-^{\frac{1}{6}})\,(B_+^{\frac{1}{2}} - B_-^{\frac{1}{2}}) \geqslant 0. \tag{73}$$

The growth rate is given by

$$\Delta_i = \frac{\sqrt{3}}{2}\,(B_+^{\frac{1}{3}} - B_-^{\frac{1}{3}}). \tag{41}$$

Along the stability boundary k_B (i.e. $\Delta_i = 0$), we have

$$\beta^2 = 0, \tag{D-1}$$

while along $a = 0$ curve ($k_\pm^a$ in Fig. 6) , we find from Appendix E that

$$B_+ = b,\ B_- = 0, \tag{D-2}$$

such that

$$\alpha^2 = \frac{3}{2}\,\beta^2. \tag{D-3}$$

On k_o^b (i.e. $\partial b/\partial k = 0$ from Eq. (54)), we have from Eq. (74)

$$a = 0 \text{ or } \beta^2 = 0, \tag{D-4}$$

which corresponds to

$$k = k_{\pm}^{a} \text{ or } k = k_B. \tag{D-5}$$

This means that $\partial\Delta_i/\partial k = 0$ curve intersects with k_o^b line at k_B and $k_{\pm}^a$ (see Fig. 6). When $\partial b/\partial k \neq 0$, we get from Eqs. (53), (54) and (74),

$$\left| a \frac{\partial a}{\partial k} \right| \sim \eta, \tag{D-6}$$

which means that the $\partial\Delta_i/\partial k = 0$ curve is close to $a = 0$ ($k_{\pm}^a$ in Fig. 6) or to $\partial a/\partial k = 0$ (k_o^a) with difference of order of η. The sign considerations (Eqs. (57)-(60)) show that

$$\frac{\partial \Delta_i}{\partial k} = 0, \quad \begin{cases} k \lesssim k_+^a \\ k_+^a > k \gtrsim k_o^a \\ k_o^a > k \gtrsim k_o^b \\ k_o^b > k \gtrsim k_-^a \end{cases}, \tag{D-7}$$

which indicate that there are two unconnected $\partial\Delta_i/\partial k = 0$ curves separated by k_o^a curve (Fig. 7). For region between the stability boundary (k_B) and R_o along k_o^b (Fig. 7), we have

$$\left| a \frac{\partial a}{\partial k} \right| \sim \epsilon_k^2, \quad \left| \frac{\partial b}{\partial k} \right| \sim \eta \, \epsilon_k, \tag{D-8}$$

where ϵ_R is the R-distance of $\partial\Delta_i/\partial k = 0$ curve from R_o, and ϵ_k is the k-distance of $\partial\Delta_i/\Delta k = 0$ curve from k_o^b. If ϵ_R is given by

$$\epsilon_R \sim \eta^{\delta}, \tag{D-9}$$

than from Eq. (D-8)

$$\epsilon_R \sim \eta^{2\delta - 1}. \tag{D-10}$$

This is interpreted that as $\partial\Delta_i/\partial k = 0$ curve moves from $k_{\pm}^a$ toward k_B, it slowly rises in k-direction and sharply decreases down to k_o^b at k_B as shown in Fig. 8.

The curve $\partial\Delta_i/\partial R = 0$ is defined by

$$\frac{\partial b}{\partial R} \alpha^2 = a \frac{\partial a}{\partial R} \beta^2, \tag{76}$$

where

$$\frac{\partial a}{\partial R} = \gamma_z^2 \frac{1}{\Omega_s R^3}, \tag{62}$$

$$\frac{\partial b}{\partial R} = -\eta \frac{(\Omega_s^2 - k^2)}{\Omega_s R^3} \frac{(s^2 - X_L^2)}{X_L} \frac{J_s(X_L)}{J_s'(X_L)}. \tag{63}$$

From Eqs. (62) and , (65) of Appendix C, we have

$$\frac{\partial b}{\partial R} < 0, \quad \frac{\partial a}{\partial R} > 0. \tag{D-11}$$

In particular, we note that

$$\left|\frac{\partial b}{\partial R}\right| \sim \eta, \tag{D-12}$$

which indicates from Eq. (76) that

$$|a| \sim \eta. \tag{D-13}$$

With sign considerations (Eqs. (57)-(60)), we conclude that $\partial\Delta_i/\partial k = 0$ curve lies to the left of $k_\pm^a$ curve with difference R-direction in the order of η. This is illustrated in fig. 9.

Appendix E. Growth Rates Along $k_\pm^a$

In this Appendix we will obtain the expression for the growth rate along $k_\pm^a$ curve (see Fig. 7) where $a = 0$. The growth rate Δ_i is given by

$$\Delta_i = \frac{\sqrt{3}}{2}\left(B_+^{\frac{1}{3}} - B_-^{\frac{1}{3}}\right), \tag{41}$$

where

$$B_\pm \equiv \frac{b}{2} + \frac{a^3}{27} \pm d, \tag{42}$$

$$d^2 \equiv b\left[\frac{b}{4} + \frac{a^3}{27}\right]. \tag{43}$$

along $k_\pm^a$ [i.e. $a = 0$ (Eq. (15))], it can be shown that

$$d = \frac{b}{2}, \; B_+ = b, \; B_- = 0, \tag{E-1}$$

and the growth rate (Eq. (41)) is given by

$$\Delta_i|_{k_\pm^a} = \frac{\sqrt{3}}{2}\,(b)^{1/3}|_{k_\pm^a} \tag{E-2}$$

Next we find the expression for b along $k_\pm^a$. With the substitution of $k = k_\pm^a$ into the expression of b (Eq. (52)), we obtain with the definitions (17) and (18),

$$b|_{k_\pm^a} = \frac{\eta}{2R^4}\,\frac{1}{[1 \pm \beta_z\,(1 - 1/R^2)^{1/2}]}. \tag{E-3}$$

Therefore we get the expression of the growth rate on $k_\pm^a$,

$$\Delta_i|_{k_\pm^a} = \frac{\sqrt{3}}{2}\left[\frac{\eta}{2R^4\,\{1 \pm \beta_z\,(1 - 1/R^2)^{1/2}\}}\right]^{1/3}. \tag{E-4}$$

In particular, when $R = R_o$ (Eq. 61)

$$R_o = \left[\frac{\gamma_z + 1}{2}\right]^{1/2}, \tag{61}$$

and $k = k_o^b = k_-^a$ $(R = R_o)$ (see Fig. 7), we have

$$\Delta_i|_{R_o,\,k_o^b} = \frac{\sqrt{3}}{2}\left[\frac{2\eta\,\gamma_z}{(\gamma_z + 1)^2}\right]^{1/3}. \tag{E-5}$$

Here we have made use of the relation

$$1 - \frac{1}{R_o^2} = \left[\frac{\gamma_z - 1}{\gamma_z\beta_z}\right]^2. \tag{E-6}$$

The expression for η is given by Eq. (48)

$$\eta \equiv \frac{2\nu\gamma_z^2\beta_\perp^2}{\gamma_o N_{in}}\,[J_{s-1}\,(X_o)\,J_s'\,(X_L)]^2, \tag{48}$$

where

$$X_L \equiv \frac{\gamma_z\beta_\perp}{R}\,s. \tag{13}$$

When $R = R_o$ (Eq. (61)), the argument of Bessel function $J_s'(X_L)$ becomes

$$\hat{X}_l \equiv s\left[\frac{2\beta_\perp^2\,\gamma_z^2}{\gamma_z + 1}\right]^{1/2}, \tag{84}$$

and $\eta\ (R_o)$ can be now written as

$$\eta(R_o) = \frac{\nu}{\gamma_o N_{ln}} \frac{\hat{X}_L^2}{s^2} (\gamma_z + 1) [J_{s-1}(X_o) J_s'(\hat{X}_L)]^2. \tag{E-7}$$

Upon substitution of Eq. (E-7), the growth rate at $R = R_o$ (Eq. (E-5)) becomes

$$\Delta_i|_{R_o, k_o^b} = \frac{\sqrt{3}}{2} \left[\frac{2\nu}{\gamma_o N_{ln}} \frac{\gamma_z}{(\gamma_z + 1)} \left\{ \frac{\hat{X}_L}{s} J_{s-1}(X_o) J_s'(\hat{X}_L) \right\}^2 \right]^{1/3}. \tag{83}$$

Appendix F. Asymptotic Behavior of $J_s'(s\xi)$

In this appendix, we will find an asymptotic expression for Bessel function $J_s'(X)$, where the argument X is given in the form of

$$X = s\xi. \tag{C-1}$$

Note that $J_s'(X_L)$, which appears frequently in the growth rate equation (e.g. Eq. (105)), is of this type, when X_L is given by Eq. (13) (or Eq. (84)). The order of Bessel function s is assumed to be integer greater than zero. By series representation, Bessel function $J_s'(X)$ can be expressed as

$$J_s'(X) = \frac{1}{2} \left(\frac{X}{2} \right)^{s-1} \sum_{k=0}^{\infty} T_s^k, \tag{C-2}$$

where the kth term T_s^k is defined by

$$T_s^k \equiv (-1)^k \frac{(2k + s)}{k!\,(s + k)!} \left(\frac{X}{2} \right)^{2k}. \tag{C-3}$$

If we define the ratio of consecutive $|T_s^k|$'s as r_s^k, namely,

$$r_s^k \equiv \frac{|T_s^{k+1}|}{|T_s^k|} = \frac{(2k + s + 2)}{(k + 1)(s + k + 1)(2k + s)} \left\{ \frac{X}{2} \right\}^2, \tag{C-4}$$

then it can be shown that

$$r_s^o = \frac{s + 2}{s(s + 1)} \left(\frac{X}{2} \right)^2, \tag{C-4}$$

and

$$r_s^{k_1} > r_s^{k_2} \text{ if } k_1 > k_2. \tag{C-5}$$

Therefore, we conclude that

$$J_s'(X) \simeq \frac{1}{2} \frac{1}{(s-1,!} \left(\frac{X}{2}\right)^{s-1} \tag{C-6}$$

if

$$r_s^0 << 1 \tag{C-7}$$

The expansion condition (C-7) can be rewritten as, with Eq. (C-1),

$$\frac{s(s+2)}{(s+1)} \xi^2 << 4, \tag{C-8}$$

which, in turn, can be rewritten, in a stronger condition, as

$$s\,\xi^2 << 4. \tag{C-9}$$

The condition (C-9) may be violated with large ξ^2 or with large s. When condition (C-9) is satisfied, $J_s'(s\xi)$ (Eq. (C-6) with Eq. (C-1)) becomes

$$J_s'(s\xi) = \frac{1}{2}\left(\frac{\xi}{2}\right)^{s-1} f_s \tag{C-10}$$

where f_s is defined by

$$f_s \equiv \frac{s^{s-1}}{(s-1)!}.$$

We note that

$$f_1 = 1 \text{ if } s = 1, \tag{C-12}$$

$$f_s = \left[\frac{s}{\{(s-1)!\}^{1/s-1}}\right] \text{ if } s > 1, \tag{C-13}$$

and that if $s > 1$, $f_s^{\frac{1}{s-1}}$ is a slowly increasing function of s, approaching e (= 2.71828) as s increases to infinity. In fact we can approimate f_s as

$$f_s \simeq (e)^{s-1} \tag{C-14}$$

for $s \geqslant 1$. The approximation (C-14) is exact when $s = 1$, and at $s = 2$, where equation (C-14) is the worst approximation for f_s (Eq. (C-11)), the difference is 0.71828 (e-2). With approximate expression for f_s (Eq. (C-14)), $J_s'(s)$ now becomes

$$J_s'(s\xi) = \frac{1}{2}\left[\frac{1}{2}\,\xi\, e\right]^{s-1}. \tag{C-15}$$

We finally add that if X_L is given by Eq. (84), the expansion condition (C-9) is now

$$s\,\frac{\beta_\perp^2\,\gamma_z^2}{\gamma_z + 1} << 2, \tag{C-16}$$

and

$$J_s'(X_L) = \frac{1}{2}\left[e\frac{\beta_\perp\,\gamma_z}{[2(\gamma_z + 1)]^{1/2}}\right]^{s-1} \tag{C-17}$$

References

1. J. Y. Choe and S. Ahn, "Rigorous Derivation of General Dispersion Relationship for Gyrotron," NRL Memorandum Report 4041, May 1979.

Table I. Parametric Optimization of the Long Wavelength Modes.

Quantity	Optimization Condition
axial wavenumber	$\hat{k} = \frac{\gamma_{z-1}}{\beta_z} \frac{s\omega_c/\gamma_o}{c}$
wall radius	$\hat{R} = \left[\frac{\gamma_{z+1}}{2\gamma_z^2}\right]^{1/2} \frac{cX_{ln}}{s\omega_c/\gamma_o}$
beam center radius	$\hat{r}_o = \begin{cases} 0, & \text{if } s = \ln \\ R\,\frac{X_{\lvert s-l\rvert 1}}{X_{ln}}, & \text{if } s \neq l,\ X_{ln} - X_l \geq X_{\lvert s-l\rvert 1} \\ R - r_L, & \text{if } s \neq l,\ X_{ln} - X_L < X_{\lvert s-l\rvert 1} \end{cases}$
radial node number	$\hat{n} = 1$
azimuthal mode number	$\hat{l} = s$

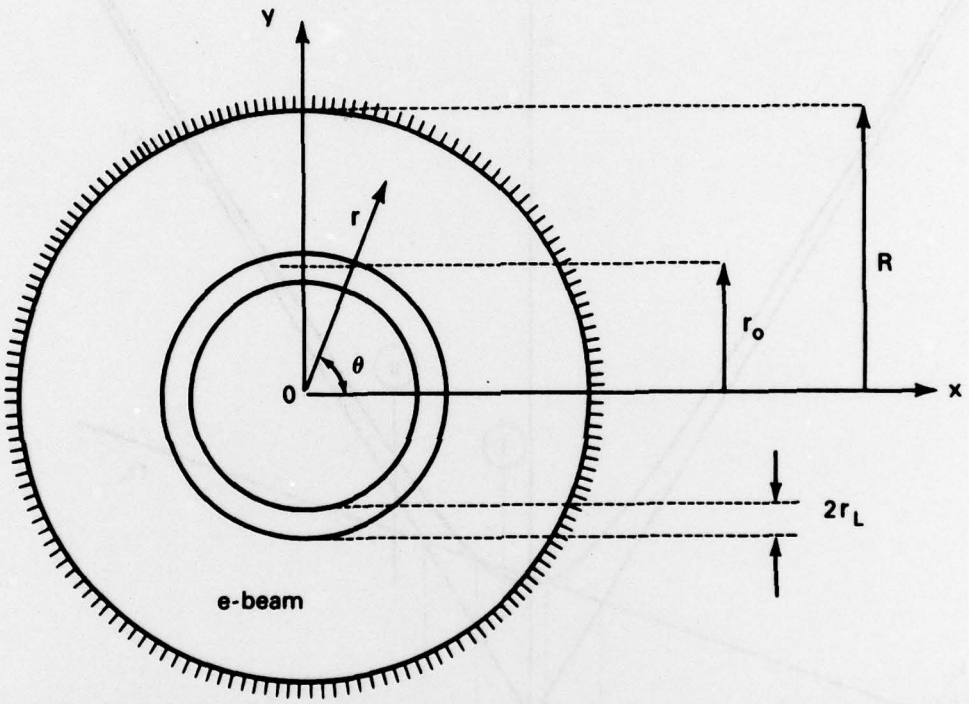

Fig. 1. Geometry of gyrotron. The beam electrons with the Larmor radii r_L and the guiding center radii r_o are contained in the cylindrical wall of radius R. The constant equilibrium magnetic field is in $\hat{e}_z$ direction (coming out of paper).

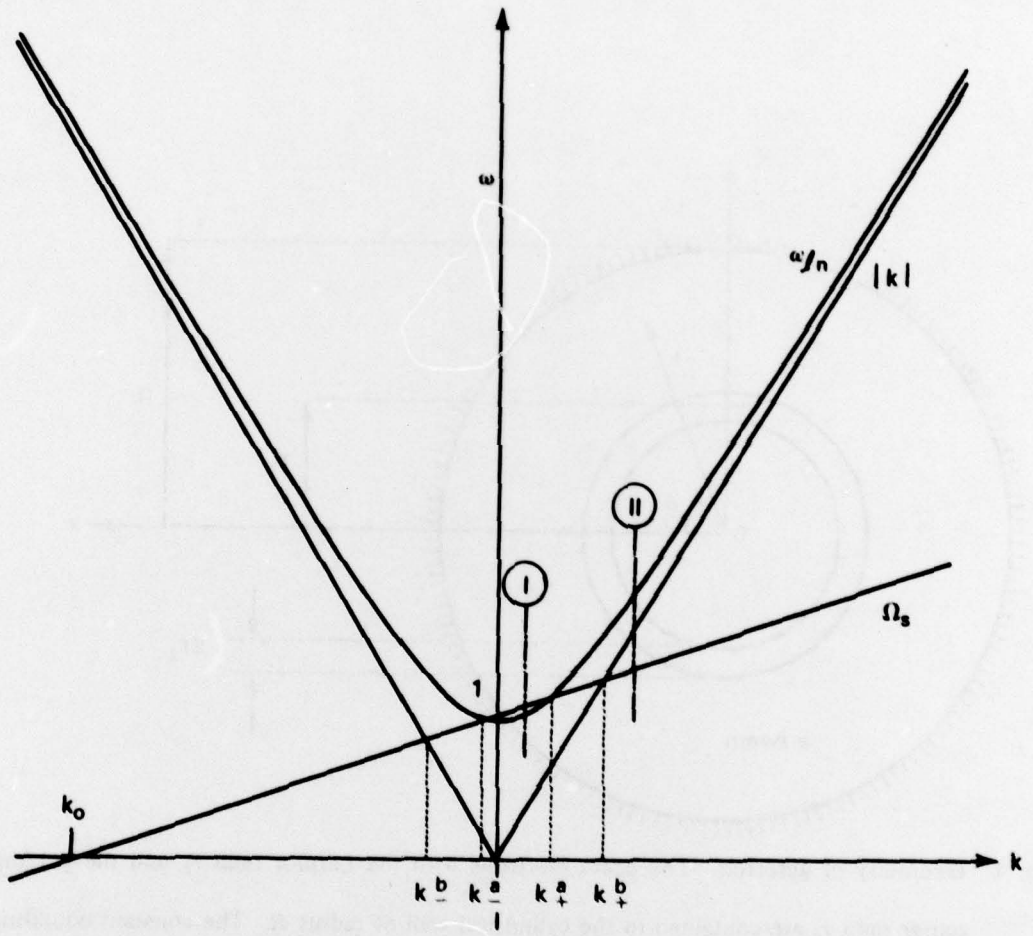

Fig. 2. Dispersion curves of the normalized waveguide (ω_{ln}) and the Doppler-shifted cyclotron motion (Ω_s) versus the norlmalized axial wavenumber k. Also shown is $|k|$ lines for reference. Note that the cutoff frequency of ω_{ln} is γ_z/R, and that $\Omega_s^2 = k^2$ at $k_\pm^b$, $\Omega_s^2 = \omega_{ln}^2$ at $k_\pm^a$, $\Omega_s = 0$ at k_o. The graph shown is for the wall radius $R > 1$. Designated as I and II are two wavenumbers at which Figs. (3a) and (3b) are drawn.

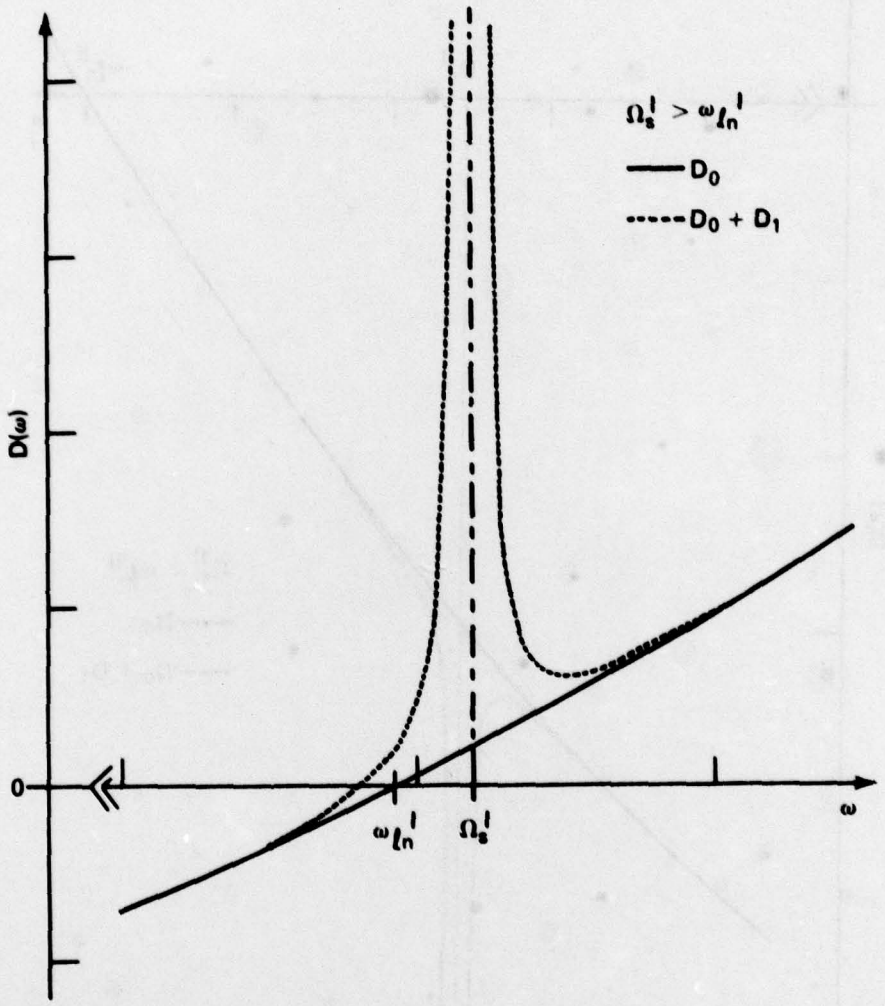

Fig. 3a. Dispersion function D versus ω near Ω_s at k' given from Fig. 2. The solid curve represents the free waveguide dispersion D_0, and the dotted approximate dispersion $D_0 + D_1$. Note that at this low k, $\Omega_s \gtrsim \omega_{\ell n}$. The local minimum near $\omega \gtrsim \Omega_s$ indicates the instability of the long wavelength mode.

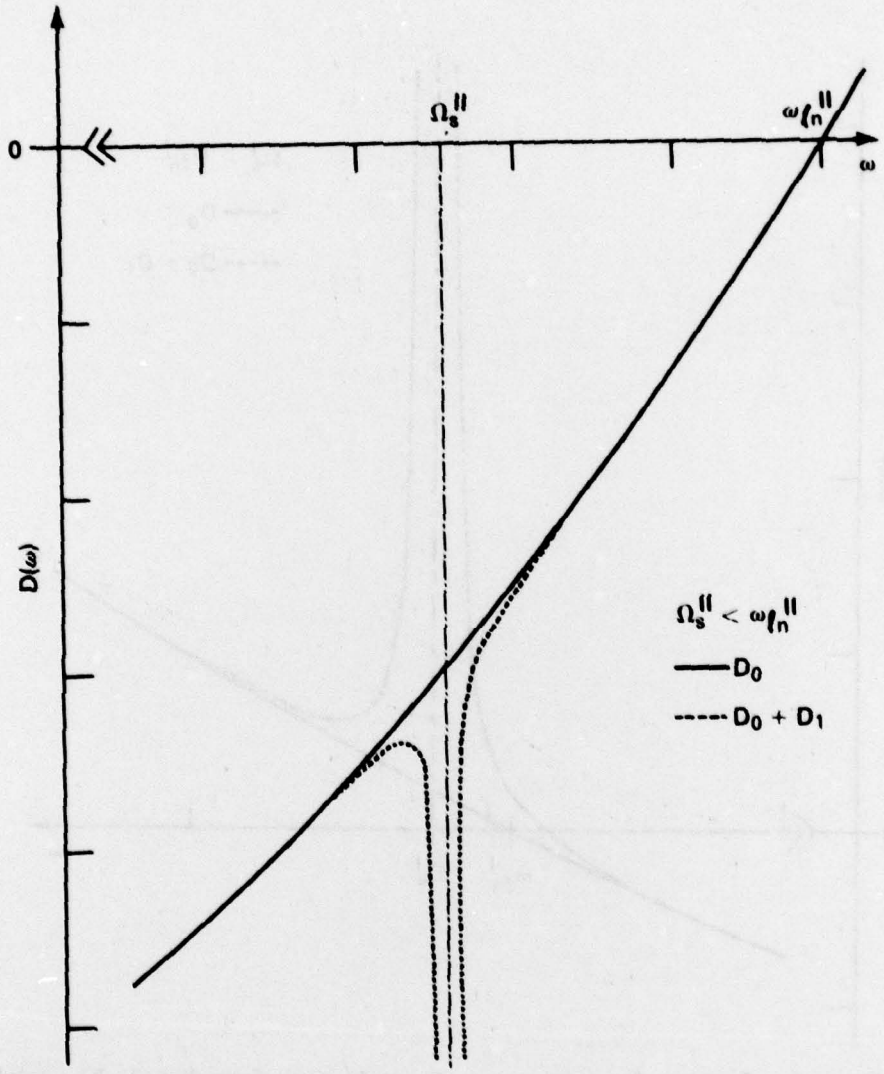

Fig. 3b. Dispersion function D versus ω near Ω_s at k^{II} given from Fig. 2. Note that at this high k, $\Omega_s < \omega_{ln}$. The local minimum near $\omega \lesssim \Omega_s$ indicates the instability of the short wavelength mode.

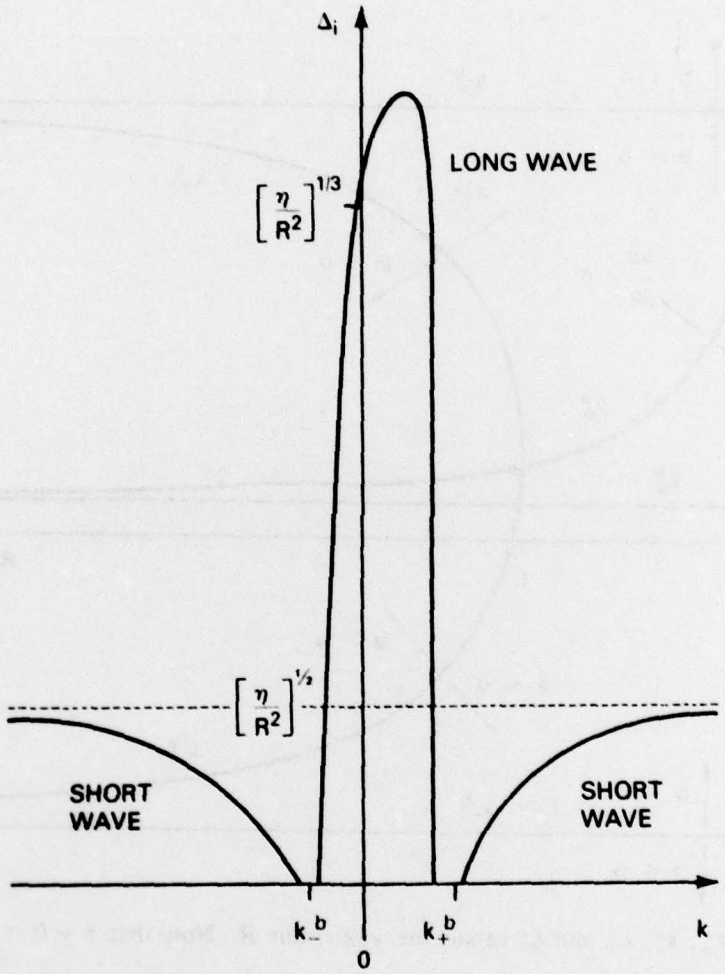

Fig. 4. Schematic plot of the growth rate Δ_i versus the axial wavenumber k. For $k < k_-^b$ and $k > k_+^b$, the short wavelength mode exists, whose growth rate monontonically increases to $[\eta/R^2]^{1/2}$ as $|k|$ increases to infinity. For $k_-^b < k < k_+^b$, the long wavelength mode is present, whose growth rate has a maximum with its magnitude in the order of $[\eta/R^2]^{1/3}$. Note that these two modes are separated by two stable regions near $k = k_\pm^b$.

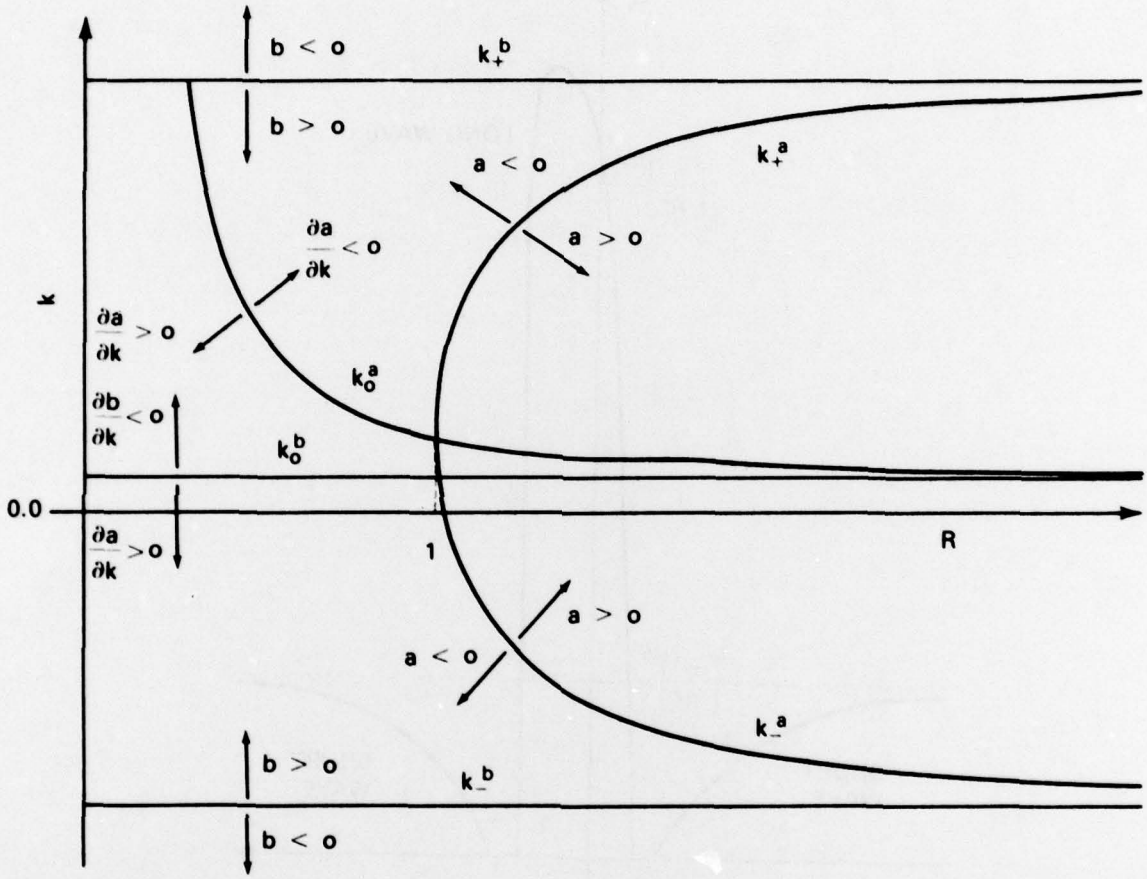

Fig. 5. Plots of $k_{\pm}^b$, k_o^b, $k_{\pm}^a$ and k_o^a versus the wall radius R. Note that $b = 0$ at $k_{\pm}^b$, $a = 0$ at $k_{\pm}^a$, $\partial b/\partial k = 0$ at k_0^b, and $\partial a/\partial k = 0$ at k_o^a (see Eqs. (53)-(60))

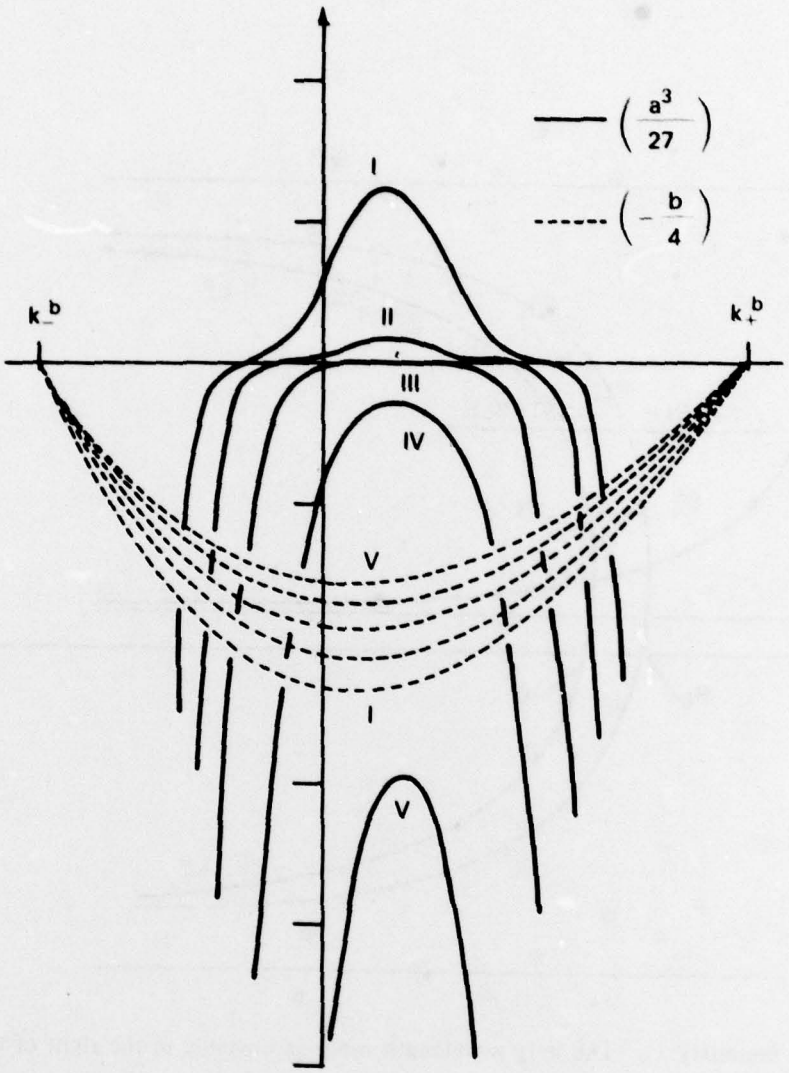

Fig. 6. Plots of $(a^3/27)$ and $(-b/4)$ versus the wavenumber k for representative wall radii designated from I to V. Here $R_I > R_{II} > R_{III} = 1 > R_{IV} > R_V$. Instability exists in k-space between the two intersecting points of the curves $(a^3/27)$ and $(-b/4)$ at each R.

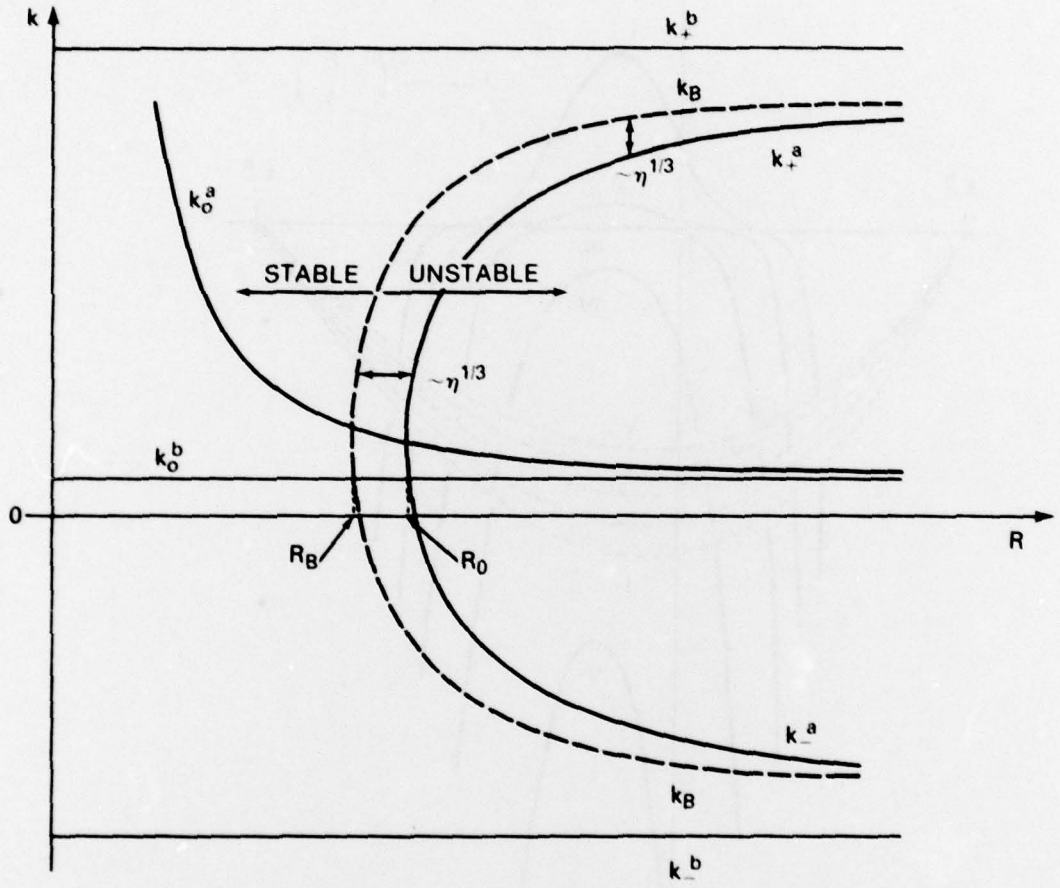

Fig. 7. Instability boundary k_B. The long wavelength mode is unstable to the right of the stability boundary k_B, on which $\Delta_i = 0$.

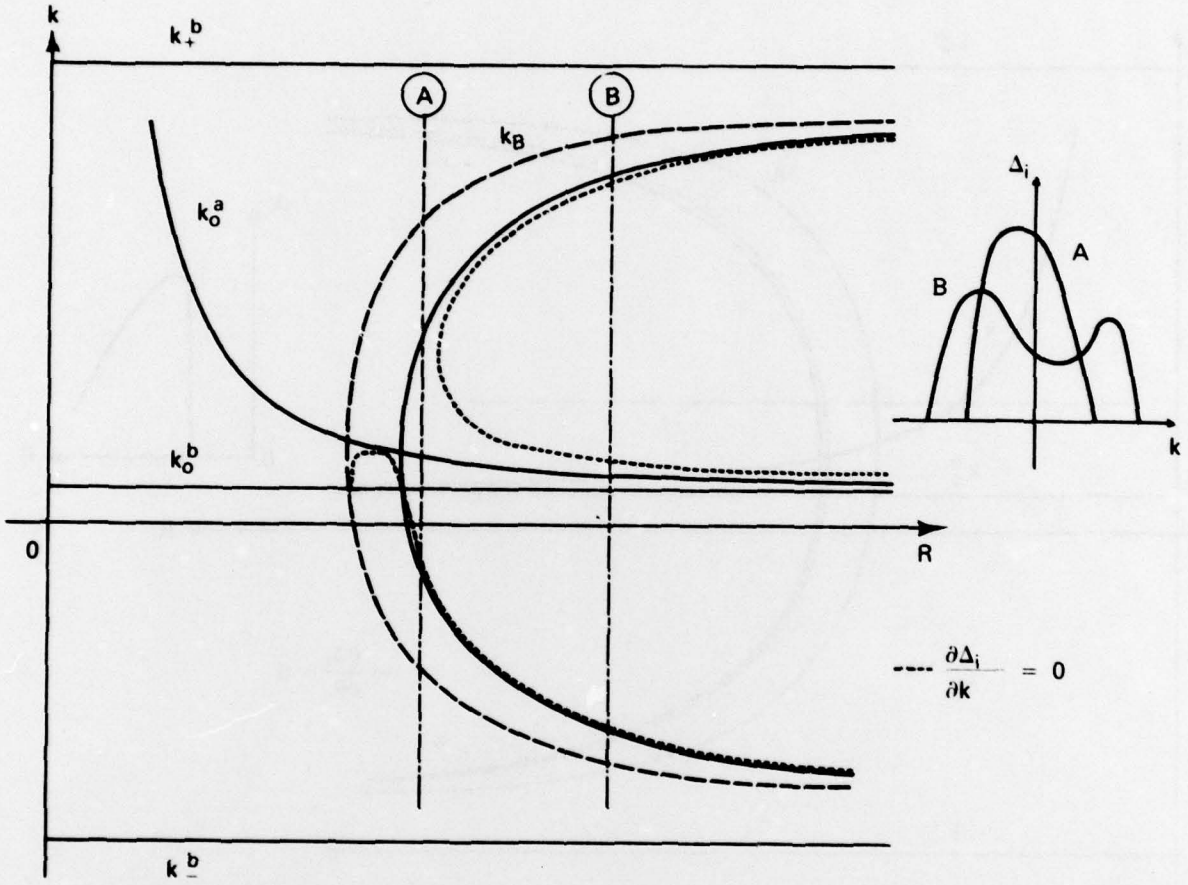

Fig. 8. $\partial \Delta_i / \partial k = 0$ curves. Also shown are the growth rate versus the axial wavenumber at two different wall radii R_A and R_B.

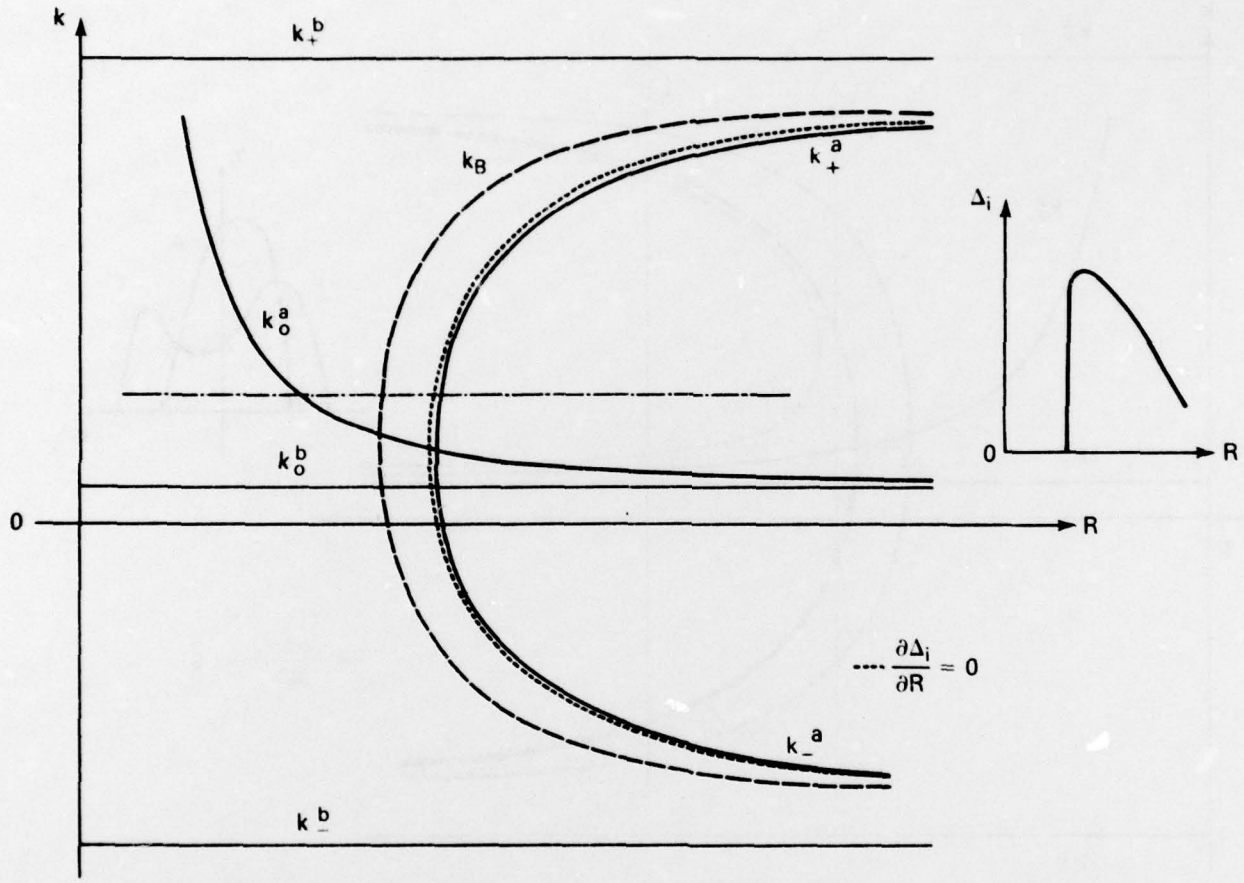

Fig. 9. $\partial\Delta_i/\partial R = 0$ curve. A representative graph of the growth rate with respect to the wall radius R at given k is also shown.

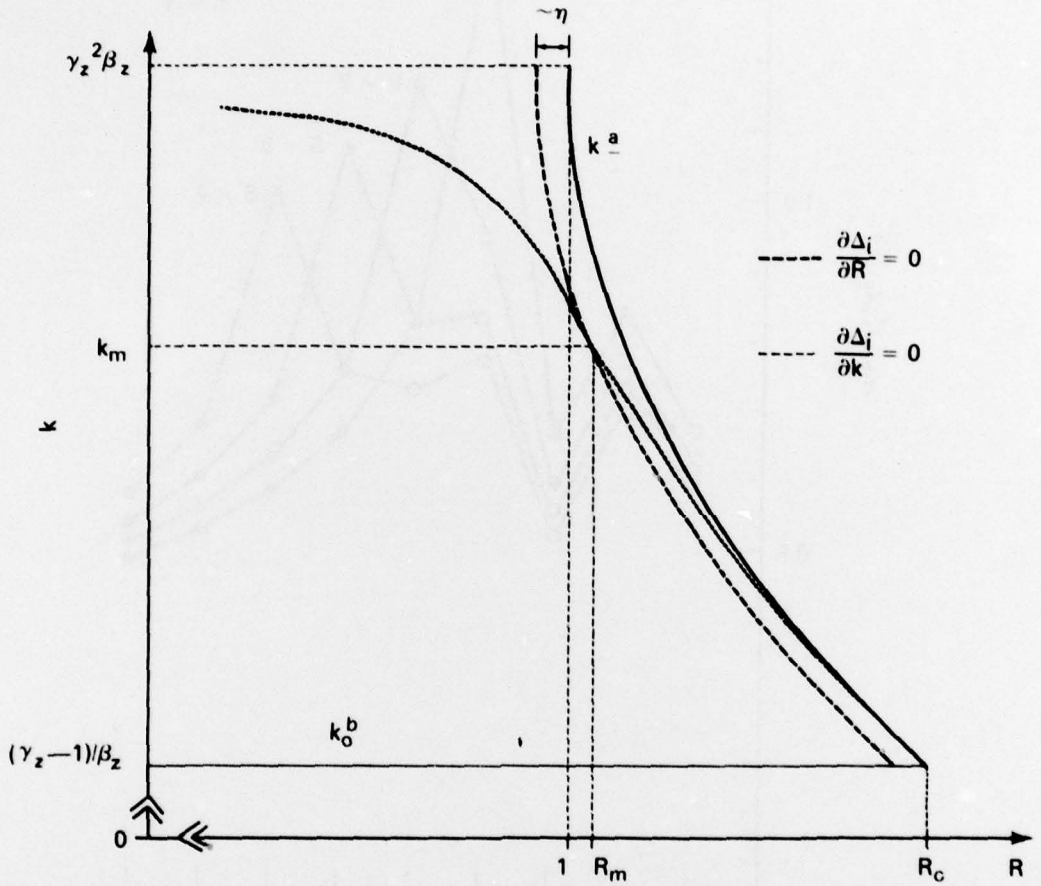

Fig. 10. Maximum growth rate in $k - R$ space. The highest growth rate occurs at the intersecting point of the curves $\partial\Delta_i/\partial k = 0$ and $\partial\sqrt{}_i/\partial R = 0$. Note that the coordinates of the point is $\sim(k_o^b,\ R_o)$.

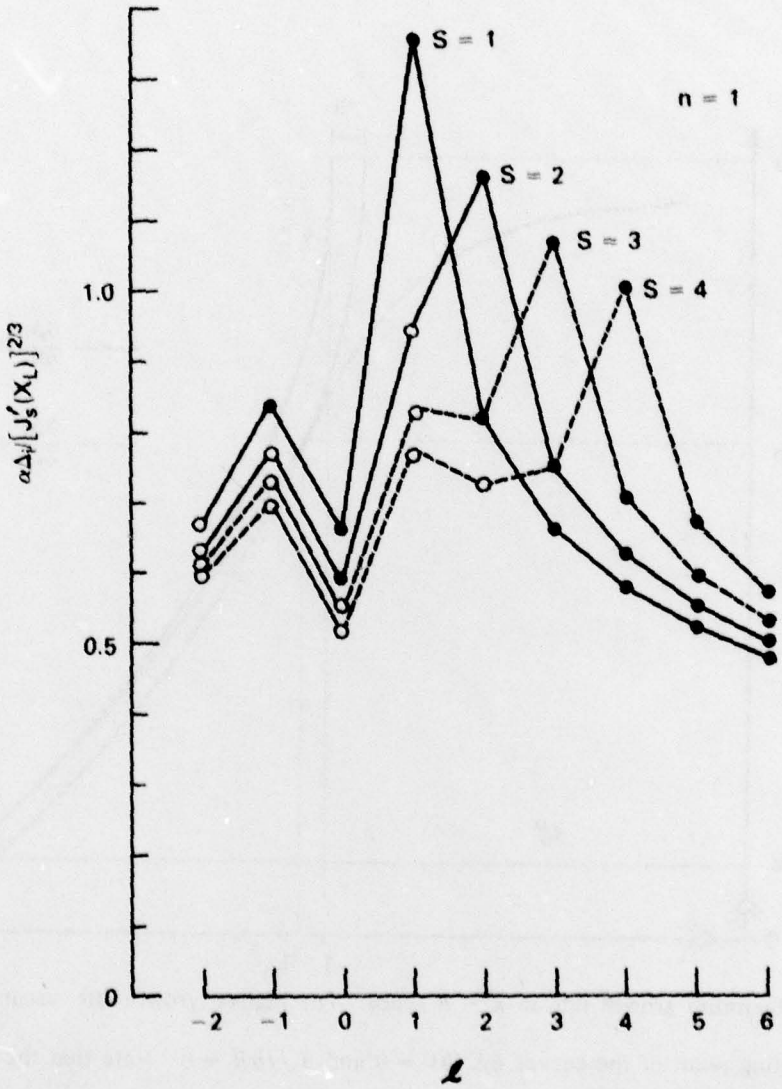

Fig. 11. Growth rate normalized by $[J_s'(X_l)]^{2/3}$ versus the azimuthal mode number l, for the magnetic harmonic number $s = 1 - 4$. Only those with the radial node number $n = 1$ are shown. The values of the growth rate are the possible maximum for given (l, s), and for those marked with open circles, the actual values are lower than those shown in the graph due to the restriction on the beam center radius (see Eq. (96-C)).

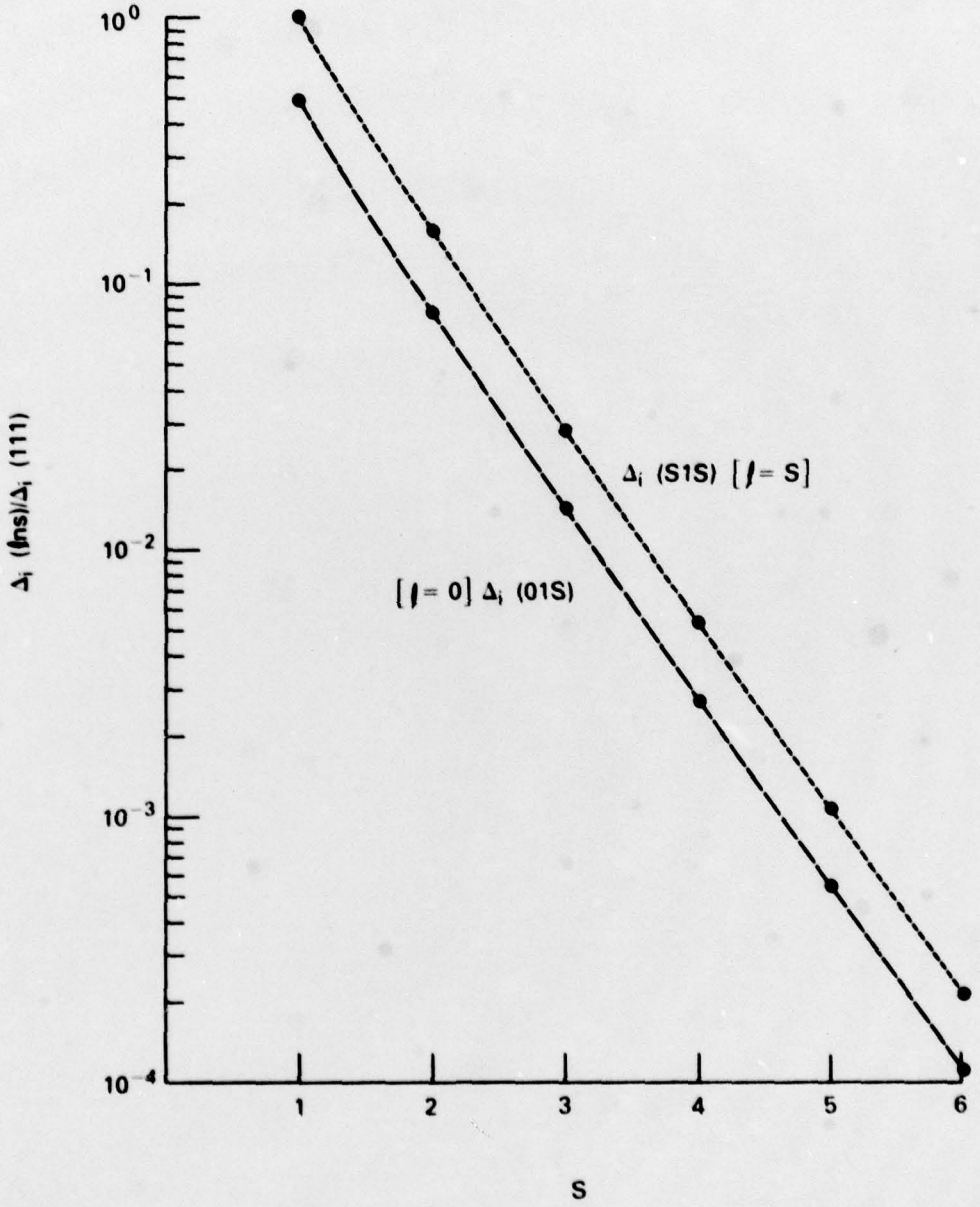

Fig. 12. Growth rate of $s = l$ mode as a function of the magnetic harmonic number s. The growth rate is normalized with that for $s = 1$.